OAK RIDGE
NATIONAL LABORATORY

MANAGED BY UT-BATTELLE
FOR THE DEPARTMENT OF ENERGY

C/ORNL98-0501

CRADA Final Report
For
CRADA No. ORNL98-0501

ADDRESSING THE MANUFACTURING ISSUES ASSOCIATED WITH THE USE OF CERAMIC MATERIALS FOR DIESEL ENGINE COMPONENTS

S. B. McSpadden, Jr.
Oak Ridge National Laboratory

R. D. Ott, T. R. Watkins,
A. A. Wereszczak, C. R. Brinkman
Oak Ridge National Laboratory

M. Andrews, B. Fix, J. Thiele
Caterpillar, Inc.

Date Published: July 2001

Prepared by
Oak Ridge National Laboratory
Oak Ridge, Tennessee 3783 1
Managed by
UT-BATTELLE, LLC
for the U.S. Department of Energy
under contract DE-AC05-00OR22725

UT-BATTELLE
ORNL-27 (4-00)

DOCUMENT AVAILABILITY

Reports produced after January 1, 1996, are generally available free via the U.S. Department of Energy (DOE) Information Bridge.

Web *site* http://www.osti.gov/bridge

Reports produced before January 1, 1996, may be purchased by members of the public from the following source.

National Technical Information Service
5285 Port Royal Road
Springfield, VA 22161
Telephone 703-605-6000 (1-800-553-6847)
TDD 703-487-4639
Fax 703-605-6900
E-mail info@ntis.fedworld.gov
Web *site* http://www.ntis.gov/support/ordernowabout.htm

Reports are available to DOE employees, DOE contractors, Energy Technology Data Exchange (ETDE) representatives, and International Nuclear Information System (INIS) representatives from the following source.

Office of Scientific and Technical Information
P.O. Box 62
Oak Ridge, TN 37831
Telephone 865-576-8401
Fax 865-576-5728
E-mail reports@adonis.osti.gov
Web site http://www.osti.gov/contact.html

CRADA Final Report
for
CRADA Number ORNL-98-0501

ADDRESSING THE MANUFACTURING ISSUES ASSOCIATED WITH THE USE OF CERAMIC MATERIALS FOR DIESEL ENGINE COMPONENTS

Compiled by
S. B. McSpadden, Jr.
Oak Ridge National Laboratory

Principal Investigators
R. D. Ott, T. R. Watkins, A. A. Wereszczak, C. R. Brinkman
Oak Ridge National Laboratory

M. Andrews, B. Fix, J. Thiele
Catepillar, Inc.

Date Published: July 2001

Prepared by the
Oak Ridge National Laboratory
Oak Ridge, TN 3783 1
Managed by
UT Battelle, LLC
For the U.S. Department of Energy
Under contract No. DE-AC05-00OR22725

*This work was supported through a CRADA with Caterpillar, Inc., Mossville, Illinois, sponsored by the U.S. Department of Energy, Office of Transportation Technologies, Heavy Vehicle Program, under contract DE-AC05-00OR22725 with Oak Ridge National Laboratory, managed by UT-Battelle, LLC.

Abstract

This CRADA supports the objective of selecting appropriate ceramic materials for manufacturing several diesel engine components and addressing critical manufacturing issues associated with these components. Materials that were evaluated included several varieties of silicon nitride and stabilized zirconia. The critical manufacturing issues that were addressed included evaluation of the effect of grain size and the effect of the grinding process on mechanical properties, mechanical performance, reliability, and expected service life.

The CRADA comprised four tasks:

1. Machining of Zirconia and Silicon Nitride Materials
2. Mechanical Properties Characterization and Performance Testing
3. Tribological Studies
4. Residual Stress Studies

Using instrumented equipment at the High Temperature Materials Laboratory (HTML) Machining and Inspection Research User Center (MIRUC), zirconia and silicon nitride materials were ground into simulated component geometries. These components were subsequently evaluated for mechanical properties, wear, and residual stress characteristics in tasks two, three, and four.

Objective

The objective of this CRADA is to select appropriate ceramic materials for manufacturing several diesel engine components and to address critical manufacturing issues associated with these components. Materials evaluated include several varieties of silicon nitride and stabilized zirconia. The critical manufacturing issues include evaluation of the effect of grain size and the effect of the grinding process on mechanical properties, mechanical performance, reliability, and expected service life.

Introduction

A major issue that has hindered the widespread use of ceramic engine components is the lack of understanding of how the material composition, processing, and surface preparation affect the performance, durability and reliability of ceramic components as compared with their traditional metal counterparts. Gaining an understanding of how these factors interact will enable a designer to specify an appropriate ceramic material composition, grain size, and surface preparation technique to optimize the reliability and durability of the ceramic component. Successful completion of this work should lead to improvements in diesel engine efficiency and durability, and reduction of emissions through the use of advanced ceramic materials in valves, cam rollers, ceramic head plates and other engine components.

This report summarizes work performed as part of a Cooperative Research and Development Agreement (CRADA) between Lockheed Martin Energy Research Corporation and Caterpillar, Inc. (During the course of the CRADA, the contractor for the Oak Ridge National Laboratory changed from Lockheed Martin Energy Research Corporation to UT-Battelle, LLC.) In this cooperative research project, both ORNL and Caterpillar made critical contributions. This project would not have been possible without the intensive participation of both organizations, since neither party had all the knowledge or existing skill base to successfully complete the project alone.

The CRADA comprised four research tasks that were intended to address issues in cost-effective manufacturing, mechanical properties, performance, and reliability.

Task 1 – Machining of Zirconia and Silicon Nitride Materials

This task addressed manufacturing issues associated with grinding of silicon nitride and zirconia components, Using instrumented equipment at the Machining and Inspection Research User Center (MIRUC) in the High Temperature Materials Laboratory (HTML), zirconia and silicon nitride materials were ground into simulated component geometries. These components were subsequently evaluated for mechanical properties, wear, and residual stress characteristics in tasks two, three, and four.

Task 2 – Mechanical Properties Characterization and Performance Testing

In this task, mechanical prop&-ties issues were investigated, including mechanical performance, fatigue and corrosion analysis, and service life prediction. Activities included mechanical properties characterization and performance testing of zirconia and silicon nitride materials at room temperature and in extreme operating environments. This effort also included characterization of strength, slow crack growth susceptibility, dynamic fatigue testing, life prediction, and mechanical reliability analysis.

Task 3 – Tribological Studies

This task addressed performance issues including repeated impact wear and damage assessment. Plans called for much of the repeated impact work to be done on equipment at ORNL, while other tribological studies including scuffling resistance tests were to be performed at Caterpillar facilities. The task was intended to supplement previously reported scuffing resistance studies performed by Michael H. Haselkorn both at ORNL and at Caterpillar. By mutual agreement, this task was discontinued early in the project, and effort was directed toward the other three tasks.

Task 4 – Residual Stress Studies

In this task residual stresses were measured in various parts of interest to allow generation of "process performance maps," showing residual stress as a function of a performance metric. Residual stress studies were conducted to determine the effect of'machining (grinding) process variables on the sub-surface condition of the component.

Presentation of Experimental Work

Principal investigators for each of the completed tasks made individual contributions to this final report to summarize the work for that task. The writing style varies slightly among the contributors, and there is some overlap of technical content where interaction occurred between two or more tasks.

Task 1 – Machining of Zirconia and Silicon Nitride Materials

Creep feed machining of GS-44 Si_3N_4

A study was performed to evaluate the surface machining effects on the strength and resulting residual stress on AlliedSignal's gelcast GS-44 Si_3N_4. A Nicco instrumented creep feed grinder was used for this investigation (refer to Table 1 for the capacities of the surface grinder). Four different machining conditions (refer to Table 2) were chosen (ASTM, Cl, C4, and C8), with increasing grinding severity, one of which was the ASTM C 116 1 condition. The bars machined under the ASTM condition were used as a strength comparison for other MOR bars that had been machined under similar conditions at Chand Kare'. All the MOR bars were machined transversely, except for the ASTM bars. The Grit Depth of Cut (GDC) is a variable that encompasses most of the important machining parameters into one convenient term,

$$t = \sqrt{\frac{V_t}{V_w C}\left(\frac{d}{D}\right)^{1/2}}$$

[1] Chand Kare Technical Ceramics, 2 Coppage Drive, Worcester, MA 01603

where,

t = grit depth of cut (mm)

V_t = table speed (mm/s)

V_w = wheel surface speed (mm/s)

C = diamond concentration ($\#/mm^2$)

d = depth of cut (mm)

D = wheel diameter (mm).

The grit depths of cut and the material removal rates (MRR) for the three conditions of interest (not including ASTM condition) are shown in Figure 1 and Figure 2, respectively. The higher GDC corresponds to a higher MRR, which is to be expected.

Table 1. Capacities of Nicco Creep Feed Surface Grinder.

Spindle stiffness	17,000 N/mm
Maximum RPM	3,500
Spindle power, KW (Hp)	5.6 (7.5)
Table speed range	0.004 to 17 mm/s
Down feed resolution	0.001 mm

Table 2. Machining parameters for the three main conditions of interest and the ASTM condition.

	Condition 1	Condition 4	Condition 8	ASTM
Grit size (203 mm diamond resin bonded wheel)	325/400	170/200	170/200	320
RPM (wheel surface speed, m/s)	3535 (37.6)	1880 (20)	1880 (20)	1880 (20)
Down feed, μm (total removal μm)	2.5 (100?)	100 (300)	10 (100?)	2
Cross feed (mm)	0.75	0.75	0.75	0.7
Table speed (mm/s)	17	17	16.7	200
Diamond concentration ($\#/mm^2$)	17	9	9	17

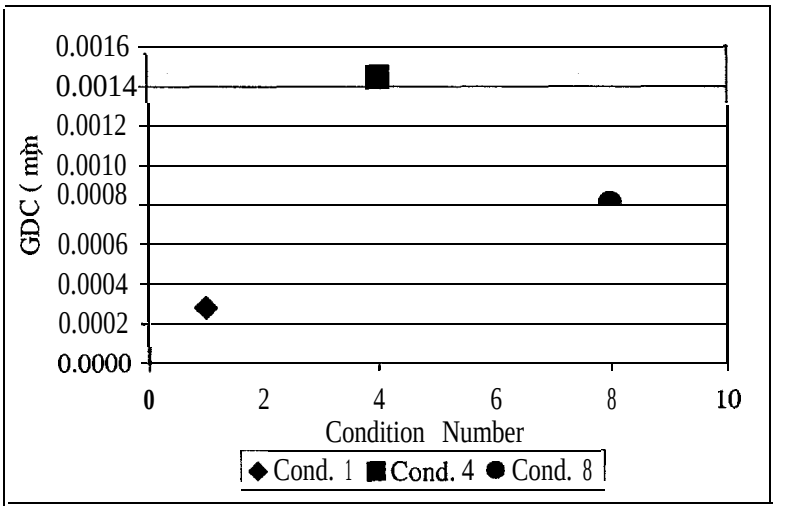

Figure 1. Grit depth of cut (GDC) for the three machining conditions (Cl, C4, and C8).

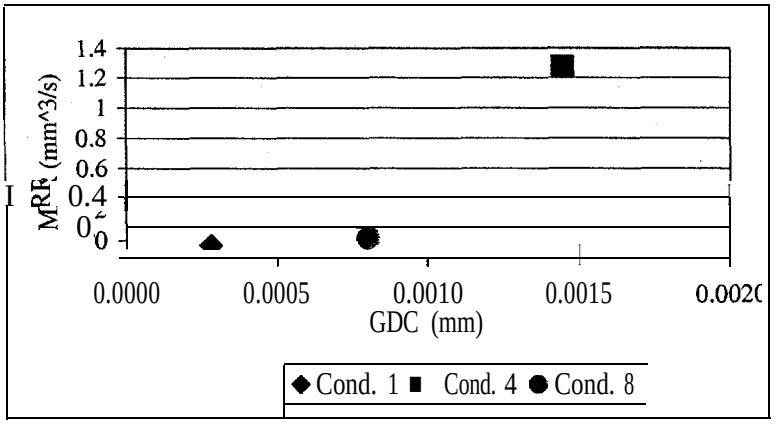

Figure 2. Material removal rate (MRR) for the three machining conditions.

Machining Process and Data Collection

During the grinding process the vertical and horizontal machining forces and the spindle power level were recorded Data were recorded twice during the experimental runs for Cl and C8 and three times for C4. The duration of each data-recording segment was approximately four minutes in order to obtain an adequate amount of data. The force and horsepower data were very consistent among the data collection periods for a given machining condition. The tangential and normal machining forces, calculated from the vertical and horizontal machining forces, for the three machining conditions are shown in Figure 3 and

Figure 4, respectively. Both the tangential and normal forces increase with increasing GDC. There is no significant difference (at 95% confidence level) among the tangential forces and the normal forces for Cl and C8.

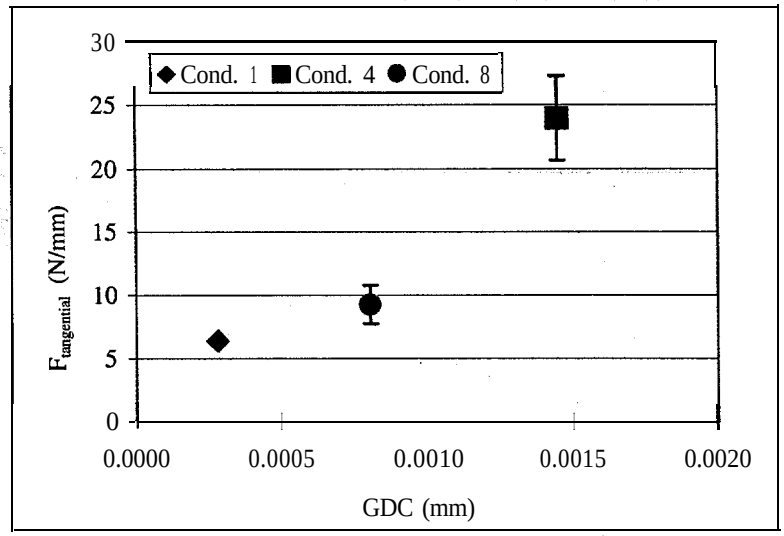

Figure 3. Tangential force vs. grit depth of cut (GDC). 'The error bars represent ± 1 standard deviation.

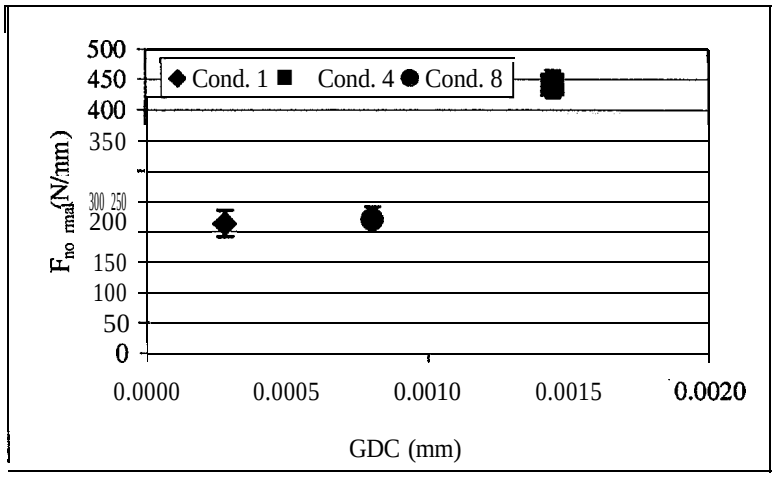

Figure 4. Normal force vs. grit depth of cut (GDC). The error bars represent ± 1 standard deviation.

The horsepower can be calculated (H_{cal}) from the tangential force (F_t in N) and the wheel surface speed (V, in m/s) by the following equation:

$$H_{cal} = 0.00134(F_t V_w)$$

The trend of the measured and calculated spindle horsepower as a function of GDC can be seen in Figure 5. The horsepower value increases with increasing GDC, following the trend of the tangential force. The calculated horsepower values for Cl and C8 are higher than the measured horsepower, which is probably due to the low level of horsepower required to remove the material and the accuracy to be able to measure such'low levels of power. The higher material removal rate and higher horsepower associated with C4 shows that the calculated and measured horsepower are more agreeable. A more significant term, which would be associated with machining cost, is the specific grinding energy (refer to Figure 6), which is the ratio of the horsepower to the material removal rate. As can be seen the specific grinding energy decreases significantly with increasing GDC.

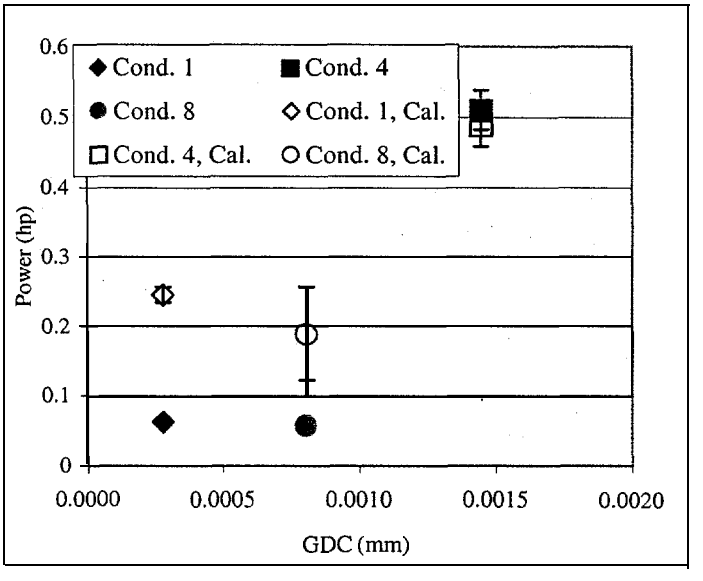

Figure 5. Measured and calculated horsepower vs. grit depth of cut (GDC). The error bars represent ± 1 standard deviation.

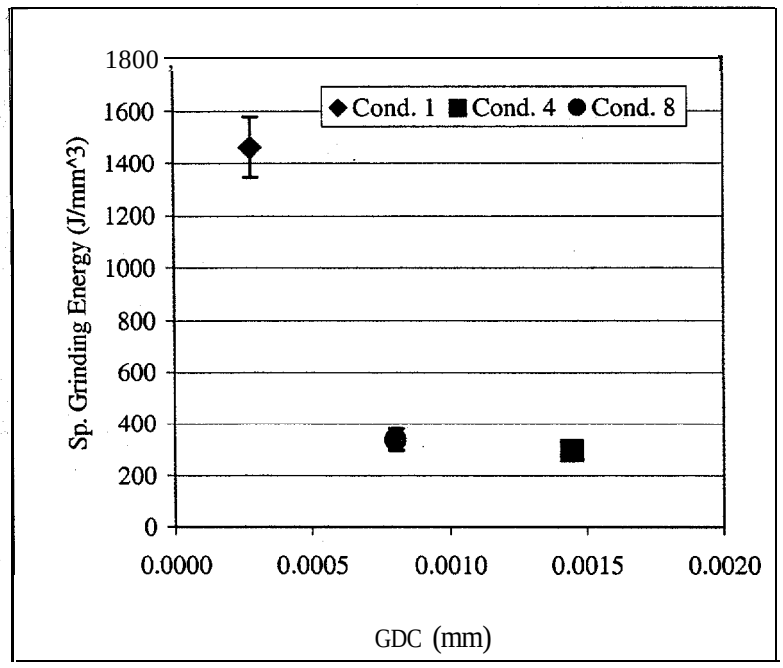

Figure 6. Specific grinding energy vs. the grit depth of cut (GDC). The error bars represent ± 1 standard deviation.

Surface Roughness

The surface roughness of specimens machined according to the conditions Cl, C4 and C8 were measured perpendicular to the machining direction. Four surface roughness parameters were measured: R_a (arithmetic mean of the departures of the roughness profile from the mean line), R_q (root-mean-square), R_t (maximum peak to valley height of the profile), and R_z (average height difference between the five highest peaks and the five lowest valleys). The values for these parameters are shown in Figure 7, Figure 8, Figure 9, and Figure 10, respectively. As can be seen, C4 produces the lowest surface roughness among the three conditions. This is thought to be due to the fact that fewer passes were used to remove the material on the experimental surface, thus reducing the amount of contact between the experimental surface and the grinding wheel. As the number of contacts increases a profile is likely to build up on the wheel, and the profile is transferred to the experimental surface causing the surface roughness to increase. By comparing C4 and C8 (the only difference being the down feed and the amount of contact between the experimental surface and the grinding wheel) it can be seen that the surface roughness increased in condition C8. This is most likely because of the higher number of passes required to remove the material in condition C8. This behavior is even more evident in the surface profiles for the three different conditions shown in Figure 11. The wheel cross feed, of 0.75 mm, is quite evident in the surface profile of C8 and somewhat in C4.

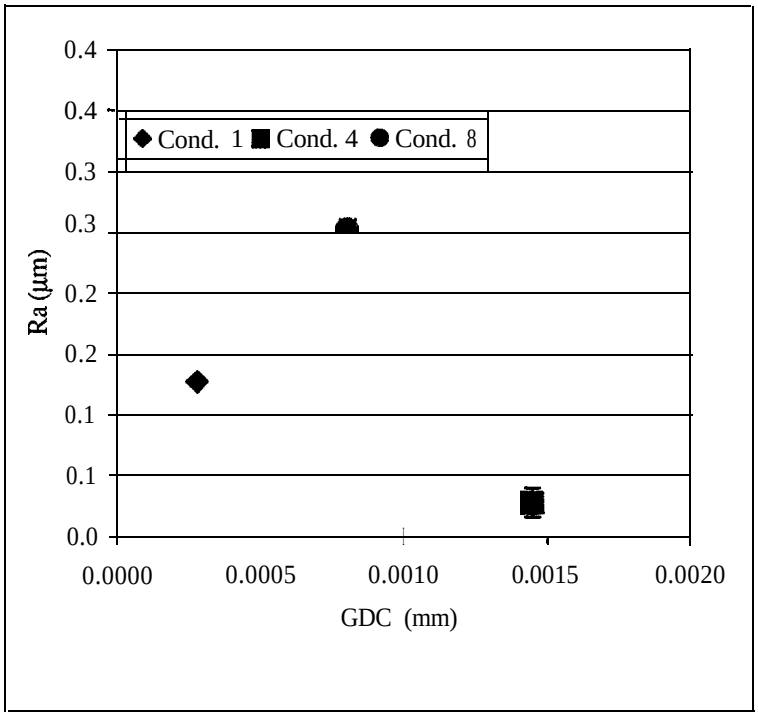

Figure 7. Ra surface roughness for the three different machining conditions. The error bars represent ± 1 standard deviation.

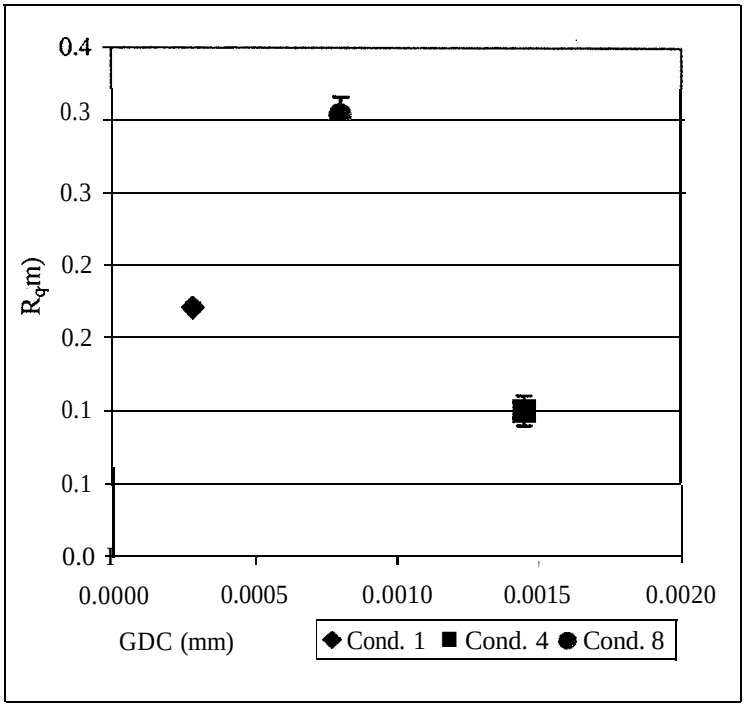

Figure 8. R_q (RMS) surface roughness for the three different machining conditions. The error bars represent ± 1 standard deviation.

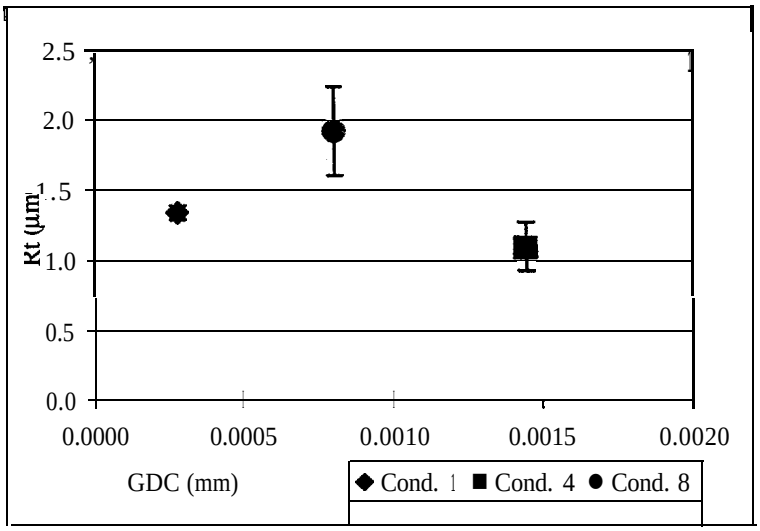

Figure 9. Rt surface roughness for the three different machining conditions. The error bars represent ± 1 standard deviation.

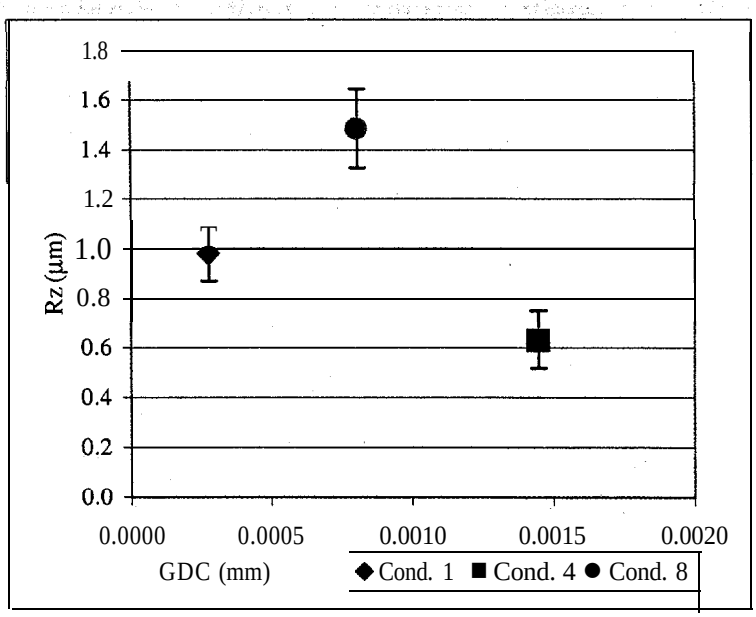

Figure 10. Rz surface roughness for the three different machining conditions. The error bars represent ±1 standard deviation.

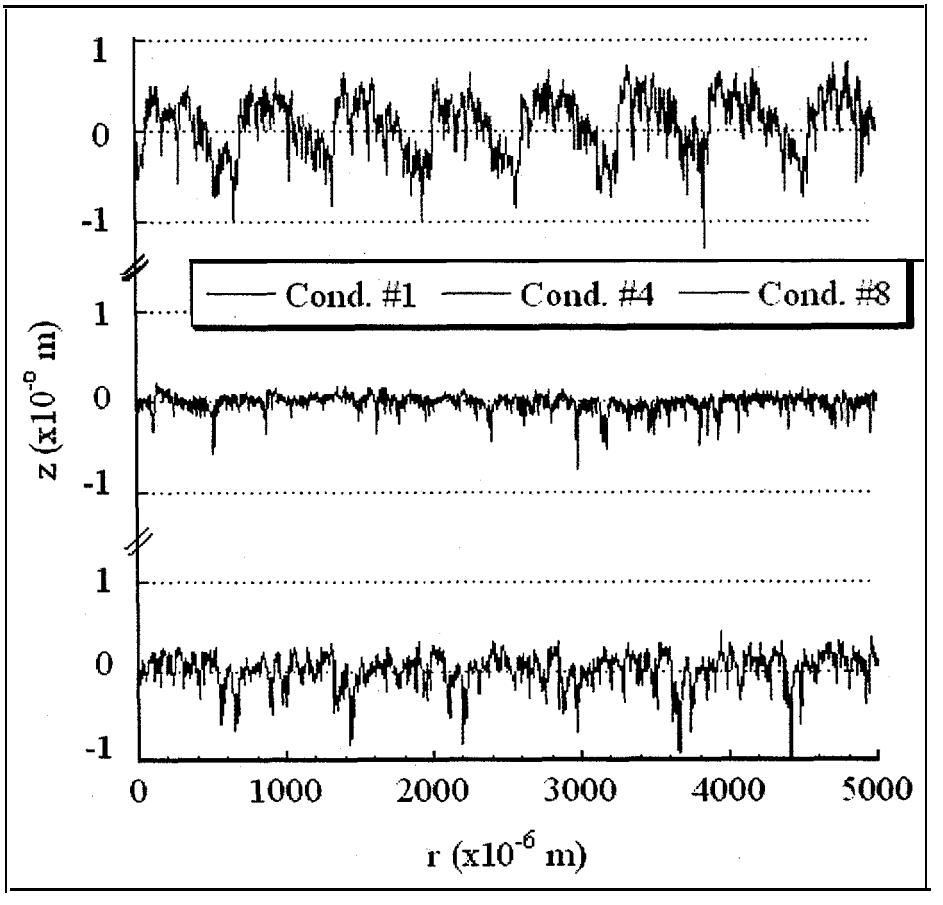

Figure 11. Surface roughness profiles for the three different machining conditions.

Residual Stresses

(Work reported in this section was performed by Thomas Watkins, ORNL.)

Residual stresses were measured for samples machined under conditions Cl and C8 using grazing incidence x-ray diffraction with Cu Kα radiation. The residual stresses parallel to the machining direction are reported. The surface layer, consisting of machined ceramics, usually contain material that is highly plastically deformed (compressive residual stress), which is able to be measured by low angles of x-ray incidence due to the small penetration depths. In order to balance out these surface compressive residual stresses, there must be a layer of material beneath that is in tension, and beneath that lies material that is stress free. X-ray data for low angles of incidence shows that the best fit of the spectra occurs when deconvoluted into two peaks, one relating to the shallow compressive surface layer and the other relating to the volume of material that is in tension and/or stress free. These data and hypothesis are confirmed by residual stresses measured by synchrotron data, which show the presence of the compressive residual stress layer at shallow depths. This peak decreases in intensity for larger penetration depths.

Tau-profiles give the cumulative stress state at a given depth for the volume of material sampled, from the surface to that depth. They‘start with a large compressive stress and decay to zero stress as the penetration depth increases. The average stress in the volume of material sampled tends toward zero, because the compressive stresses are balanced by tensile stresses, and more and more volume’of stress free material is being sampled as penetration depth increases. T&Z-profile estimates the actual stress as a function of depth from the sample surface and is determined from the Tau-profile. The reconstructed Tau-profile determines the goodness of fit of the Z-profile. Refer to Figure 12 and Figure 13 for the Z-, Tau-, and reconstructed Tau-profiles for machining conditions C1 and C8, respectively. As can be seen the Z-profiles give a good estimate to the residual stress state of the two samples tested, as shown by the correlation of the reconstructed Tau-profile and the Tau-profile.

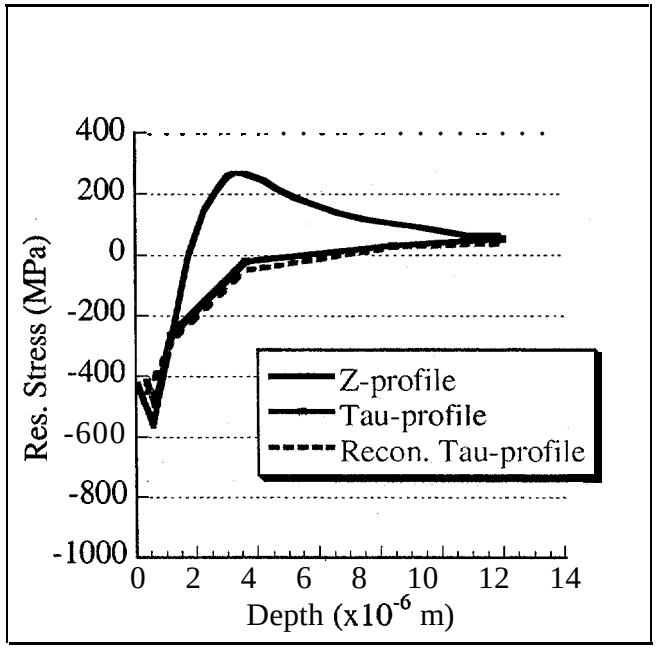

Figure 12. Residual stress profile for machining condition Cl, witb the Z-, Tau-, and reconstructed Tau-profiles.

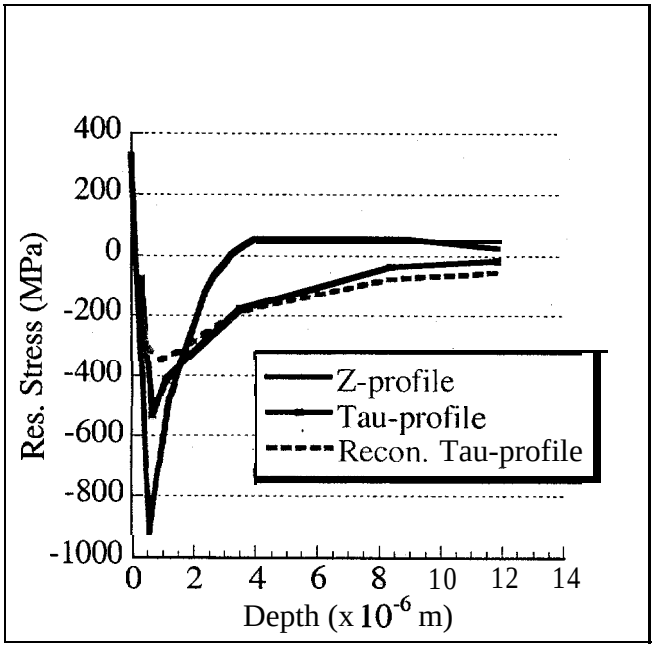

Figure 13. Residual stress profile for machining condition C8, with the Z-, Tau-, and reconstructed Tau-profiles.

Figure 14 shows the combined Tau-profiles for conditions Cl and C8, while Figure 15 shows the combined Z-profiles for the two machining conditions. It can be seen that there seems to be a lower surface compressive stress for Cl (finer grit size) than C8. The crossover from compressive to tensile stress is at a shallower depth for Cl (-1.75 μm) than for C8 (-3.25 μm). Also, specimens machined according to the Cl condition seem to have a larger tensile stress that rapidly decays to zero, where specimens machined according to the C8 condition have a lower tensile stress that slowly decays to zero. It is difficult to accurately determine the magnitude of the surface compressive stress, considering the depth of the volume of material measured is on the order of the surface roughness.

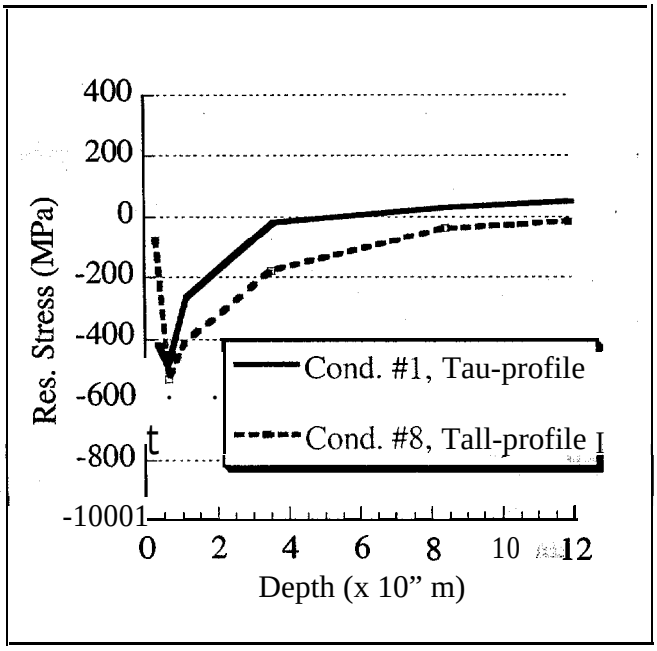

Figure 14. Combined Tau-profiles for machining conditions Cl and C8.

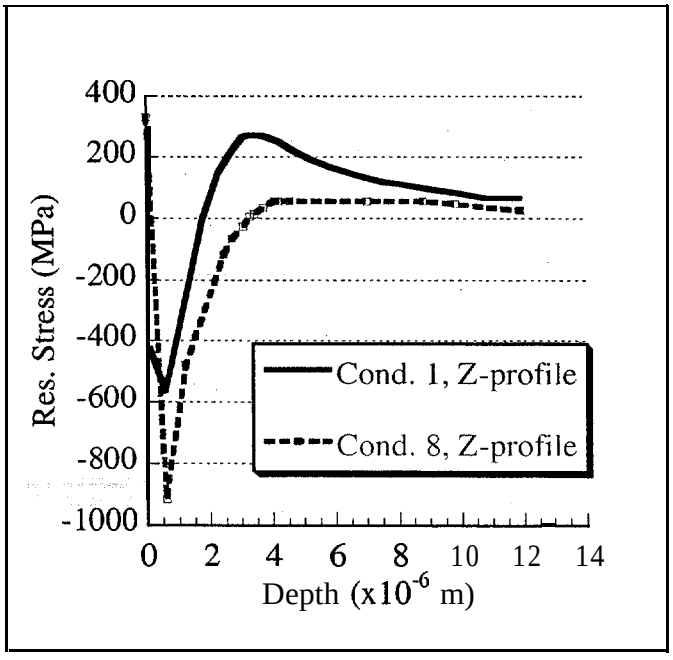

Figure 15. Combined Z-profiles for machining conditions Cl and C8, showing the depth at which the stress becomes tensile.

From these data and from previous studies, there seems to be a good correlation between the GDC and the transition depth between compression and tension, refer to Figure 16. The transition depth from compression to tension occurs deeper within the material as the GDC increases. There is also a good

correlation between the GDC and the maximum tensile stress (refer to Figure 17), with the maximum tensile strength decreasing with increasing GDC. But, there is a poor correlation with the GDC and the maximum compressive stress.

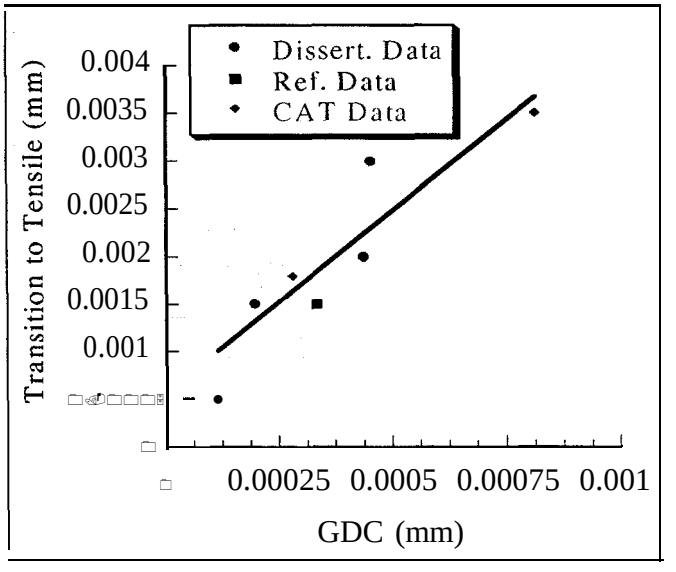

Figure 16. Depth at which the residual stress turns from compressive to tensile as a function of GDC.

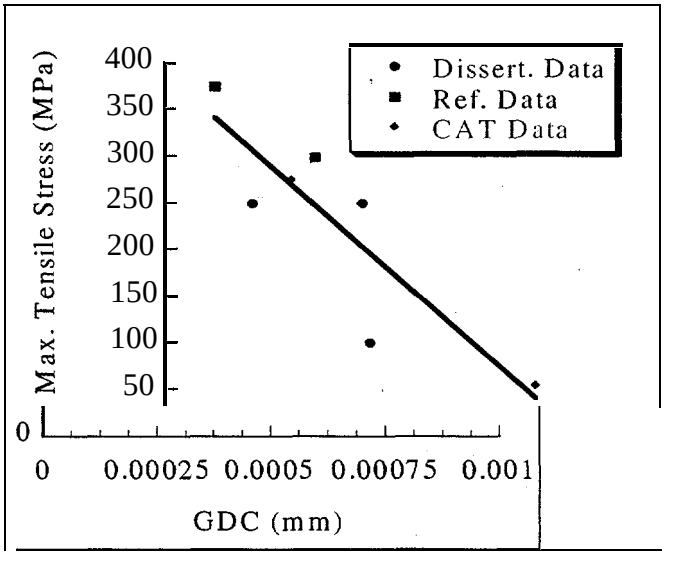

Figure 17. Maximum tensile stress as a function of GDC.

Flexure Strengths and Weibull Parameters

All the flexure bars were cut and chamfered' following ASTM Standard C 1 161, and measured and numbered. Each set of bars (from each machining condition) was randomized and 12 bars were selected from each condition (nine from ASTM condition) for room temperature fast fracture (30 MPa/s) utilizing 4-point bending. This was followed by randomization of all 45 flexure bars. The strengths were determined from the fracture loads, bar size and geometry of the 4-point bending. A significant number of the fracture surfaces were examined optically to determine the origin of failure. It looks as if all failed from surface flaws based on the mirror planes. One sample machined according to the Cl condition failed from what looked like a pore at the surface; therefore it was not censored for strength evaluation considering it was a surface flaw. It is possible the pore interacted with machining flaws to cause failure. Table 2 and Figure 18 show the average strengths for the three different machining conditions. As can be seen there is no difference in the average strengths for all three machining conditions.

Table 3. Average strengths and standard deviations for the thi-ee machining conditions and for ASTM machined flexure bars.

Cond.	Strength (MPa)	Stdev.
ASTM	849.53	81.15
C1	836.06	97.22
C4	883.66	32.56
C8	824.41	20.83

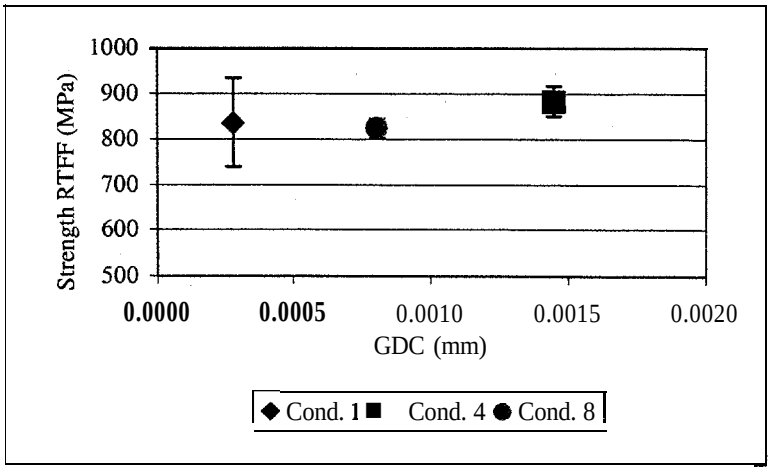

Figure 18. Room temperature fast fracture (RTFF) average strengths for the three 'different machining conditions versus the grit depth of cut (GDC).

The Weibull parameters, characteristic strength and Weibull modulus (m), are listed in Table 4. The characteristic strengths for the three machining conditions are equivalent as listed in Figure 19. Specimens machined according to conditions C4 and C8 have equivalent Weibull moduli, given the 95% confidence bounds, but are higher than the Weibull modulus for Cl (refer to Figure 20). The Weibull modulus has a tendency to increase with increasing GDC, as would be expected. An increasing GDC implies more aggressive machining, thus introducing larger (more severe) strength limiting flaws. The likelihood of a specimen failing from these larger flaws 'would be greater, therefore increasing the Weibull modulus.

Table 4. The Maximum Likelihood Weibull parameters, Weibull modulus and characteristic strength, with ±95% confidence bounds of the three machining conditions and ASTM flexure bars.

Cond.	# Spec.	Uncensored Max. Lik. Weibull m	Weibull m ±95% confidence bounds	Uncensored Max. Lik. Char. Strength (MPa)	Char. Strength ±95% confidence bounds (MPa)
ASTM	9	14.5	7.8, 23.8	883	835,930
Cl	12	14.3	8.4, 22.0	870	831,910
c4	12	34.0	20.6,51.0	898	881,915
C8	12	46.7	29.0, 68.0	834	822,845

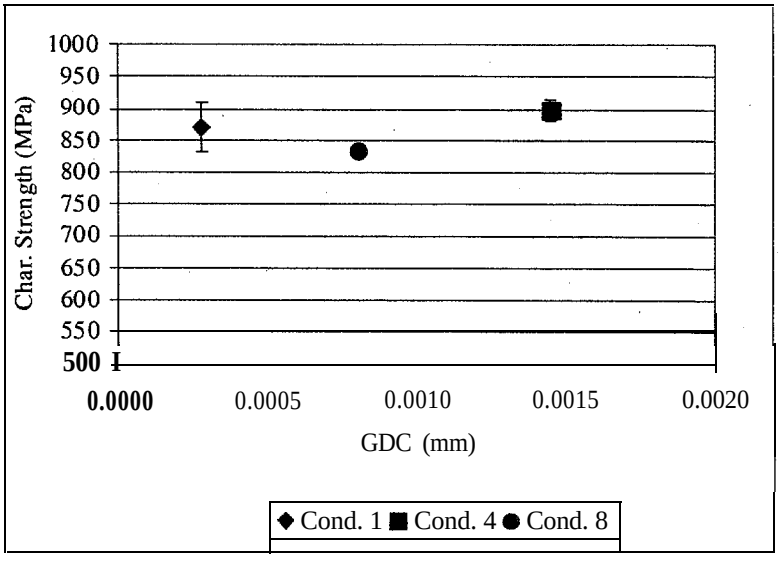

Figure 19. Maximum Likelihood Weibull Characteristic Strength for the three different machining conditions as a

function of the grit depth of cut (GDC). The error bars represent the 95% confidence bounds.

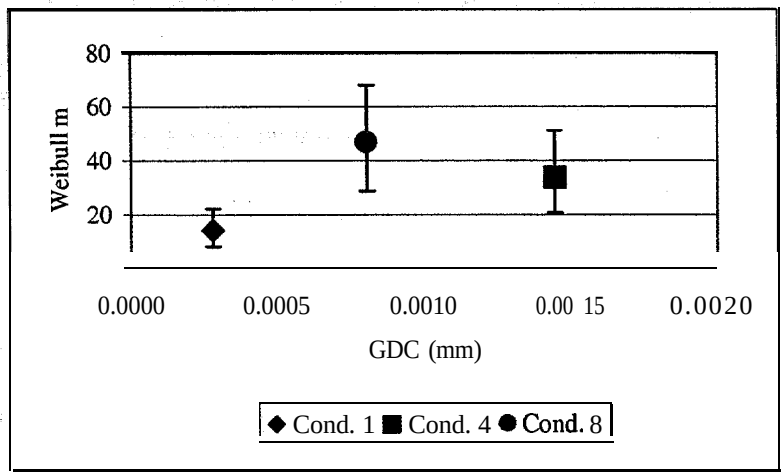

Figure 20. Maximum Likelihood Weibull Modulus for the three different machining conditions as a function of the grit depth of cut (GDC). The error bars represent the 95% confidence bounds.

Summary of Task 1

The grit depth of cut (GDC) was used to incorporate all the important machining parameters into one convenient term. The larger GDC caused an increase in the normal and tangential machining forces, as well as the spindle horsepower. The specific grinding energy which relates the amount of spindle power required for a given material removal rate (MRR) decreased with increasing GDC. At some point this value will go through a minimum and start to increase, giving the optimal machining conditions for rapid material removal.

The surface roughness was the lowest for the most aggressive machining condition (C4), which was related to the fact that fewer contacts occurred between the grinding wheel and the specimen, as seen by the surface profiles. Machining condition C4 had the largest down feed of 100 μm, an order of magnitude larger than the other two machining conditions.

The residual stress, measured for machining conditions Cl and C8, showed that as the GDC increased the transition depth between compression and tension increased, while the maximum tensile stress decreased. Evaluation of the maximum surface compressive stress is difficult given the fact that the depth at which this occurs is on the same scale as the surface roughness.

Even with the large down feed of machining condition C4, and with the other machining parameters, the machining conditions chosen for this work were not nearly aggressive enough to introduce significant strength limiting flaws. There was no statistically significant difference in the strengths for all three machining conditions. It is possible to be more aggressive (larger MRR) and still maintain high strength. Also, the Weibull modulus has a tendency to increase with increasing GDC, which would be expected due to the fact larger strength limiting flaws are being introduced at higher GDC.

Comparison of Centerless and Surface Grinding

An experiment to compare the effects of centerless and surface grinding was planned and work was started using a Harig surface grinder. Because a full-sized centerless grinder was not available, the centerless grinding process was simulated by using a DedTru® centerless grinding attachment. An attempt was made to maintain equivalent grit depths of cut between the two different machining processes, so that a direct comparison could be made based on strength. Ceradyne's silicon nitride, in billet and cylindrical forms, was used for the machining. The billets were machined under the experimental conditions and MOR bars were cut and chamfered so that they could be subsequently fractured.

The cylindrical samples were down sized from 7 mm to 4 mm. The down sizing was necessary in order to remove a layer of porosity that was formed during the processing of the samples. If this layer had not been removed, more than likely all cylindrical specimens would have failed due to the porosity and not from machining induced flaws. Unfortunately, this work had to be terminated prior to completion due to a lack of funds. The following items were not completed:

- Machine the cylindrical bar specimens to final size under the experimental conditions
- Fracture the cylindrical bar specimens
- Perform fractography and strength/Weibull analysis.
- Fracture the billet (MOR bars) specimens
- Perform strength/Weibull analysis on MOR bars

The specimens that were ground in support of this phase of Task One task will be retained for possible future use.

Task 2-Mechanical Properties Characterization and Performance Testing

Introduction

The accurate prediction of mechanical reliability and service life is a prerequisite for the successful implementation of structural ceramics as internal combustion engine components. There were three primary. goals of this research project which contribute toward that implementation: the generation of mechanical engineering data from ambient to high temperatures of candidate structural ceramics; the microstructural characterization of failure phenomena in these ceramics and components fabricated from them, and the application and verification of probabilistic life prediction methods using diesel engine components as test cases.' For all three stages, results were provided to both the material suppliers and component end-users.

The systematic study of candidate structural ceramics (primarily silicon nitride) for internal combustion engine components was undertaken as a function of temperature (< 900°C), environment, time, and machining conditions. Properties such as strength and fatigue were characterized via flexure testing.

The second goal of the program was to characterize the evolution and role of damage mechanisms, and changes in microstructure linked to the ceramic's mechanical performance, at representative engine component service conditions. These were examined using several analytical techniques including optical and scanning electron microscopy.

Lastly, numerical probabilistic models (i.e., life prediction codes) were used in conjunction with the generated strength and fatigue data to predict the failure probability and reliability of complex-shaped components subjected to mechanical loading, such as a silicon nitride diesel engine valve. The predicted results were then compared to actual component performance measured experimentally or from field service data. As a consequence of these efforts, the data generated in this program will not only provide a critically needed base for component utilization in internal combustion engines, but will also facilitate the maturation of candidate ceramic materials and a design algorithm for ceramic components subjected to mechanical loading in general.

Mechanical Property Characterization

Flexure testing of eight lots of silicon nitride was completed. This involved determining the strength distributions as a function of temperature, grinding orientation, and time (fatigue). Four-point bend flexure strengths were evaluated using ASTM-B bars (dimensions 3 x 4 x 50 mm). Testing generally occurred at

two temperatures, i.e. 20 and 850°C, and two stressing rates, i.e. 0.003 and 30 Mpa/s; and grinding orientation on the test bars was either transverse or longitudinal. All specimens were commercially finish ground with 320 diamond grit grinding for both transverse and longitudinal machining orientations according to recommended practices described in ASTM C 1161. Further, all specimens were longitudinally beveled. Limited testing was performed on test bars that had previously been exposed for 1000 h at 850°C to an oil ash environment by Caterpillar. This was done on two types of silicon nitride i.e. GS44 and SN235. The upper temperature of 850°C was selected since it is in the approximate operating temperature range of the diesel engine.

Figure 21 through Figure 24 compare uncensored characteristic strengths and Weibull modulus values for the various types of silicon nitride bars machined in either the transverse or longitudinal direction. Figure 21 and Figure 22 compare data obtained at 20°C at a stressing rate of 30 Mpa/s and indicate that bars machined in the transverse direction had on average a characteristic strength that was 14% lower than bars longitudinally machined. Characteristic strengths following 1,000 h exposure to an oil ash environment for GS44 and SN235 machined in the transverse direction are compared to unexposed strengths in Figure 21, and indicate no change in strength due to environmental exposure, Figure 23 and Figure 24 make similar comparisons for material tested at 850°C. Transverse strength at this temperature was on average 5% less than that of the longitudinally machined material.

Comparing the strength data in Figure 21 to Figure 24 for tests conducted at 20 and 850°C, it is apparent that strength generally decreased with increasing temperature, and therefore susceptibility to slow crack growth or fatigue at 850°C is a possibility. This was found to be the case when characteristic strengths were graphed as a function of stressing rate, and the fatigue exponents determined. Figure 25 and Figure 26 compare fatigue exponents for materials studied and show that most of the materials had fairly low exponents for both machining orientations. The exceptions were the SN235 and SN235P, which showed both excellent strengths and fatigue resistance. Figure 27 compares strength levels at 850°C and at a stressing rate of 0.003 Mpa/s. Comparing all the data given in Figure 21 through Figure 27, it appears that of the eight silicon nitrides examined, the SN235 appears to have the best combination of room and elevated temperature strength, and 850°C fatigue or slow crack growth resistance.

The diminished strength at 850°C below that at 20°C of AS800, GS44, KYON3000, and KYON3500, and N7202 silicon nitrides with enhanced susceptibility to slow crack growth or fatigue was attributed to a relatively high amount of sintering aid found in these materials. There was consistent evidence to suggest that if the test temperature was above the apparent softening temperature for an amorphous phase, or if the

crystalline phases in a given silicon nitride occurred below the test temperature, that the silicon nitride would show relatively poor fatigue resistance. Results from dilatometry studies were compared on all silicon nitrides studied to 900°C, and a common feature of the more fatigue resistant silicon nitrides (NT154, SN235, and SN235P) at 850°C was that their coefficients of thermal expansion showed no significant deflections below the peak test temperature of 850°C.

Weibull modulus values are not normally thought to be a function of loading rate (time) or temperature, and life prediction codes generally do not account for this possibility. Figure 28 and Figure 29 are plots of the uncensored Weibull modulus as a function of temperature and loading rate respectively. Note that two different lots of GS44 (Lots C98236 and C99091) were employed in portions of this study and showed somewhat different properties as indicated in Figure 27 and Figure 29. Most of the various types of silicon nitride plotted in Figure 28 do not indicate a significant temperature dependence of the Weibull modulus. However, the GS44 (both lots) do show some variation with temperature for the transversely machined material. Figure 29, similarly does not show a large variation in Weibull modulus values with loading rate, but there is a tendency for a slight increase with loading rate.

Figure 27 shows that when GS44 and SN235 were exposed to an oil ash environment and then tested at 850°C, there was not a significant degradation in strength due to the exposure conditions imposed. Other types of silicon nitride characterized in this program were similarly exposed, but were not subsequently tested for strength degradation nor were detailed microscopic examinations and analyses performed to analyze the corrosion products. This should be done as a future activity. The Kyocera SN235 and the Honeywell GS44 were subjected to microscopic analysis and the corrosion products characterized. In the case of the SN235, the non-protective oxide scale was found to contain Zn-Ca-P-S-Si-0 while the similar appearing scale on the GS44 was determined to contain Zn-Ca-P-S-Si-Al-Mg-0. Figure 30 and Figure 3 1 compare the fracture surfaces of these two materials and indicate that the SN235 exhibited approximately a 3-micron while the GS44 a 15-micron environmental affected zone. Reasons for these differences require further analysis.

Life Prediction of NT551 Valves

The strengths of four sets of valves were measured. Two of the sets were “as-received” sets while the other two sets were comprised of engine-tested valves; the strengths of the as-received sets were compared to the retained strengths of the engine-tested sets. The fillet radius on the valves was either longitudinally or transversely machined, and this served as an independent parameter. The engine-tested valves whose fillet

radius was longitudinally machined were engine tested at Detroit Diesel Corporation (DDC) for 166 hours. The engine-tested valves whose fillet radius was transversely machined were engine tested at DDC for 1000 hours. The strength of the as-received valves and the retained strengths of the engine-tested valves were measured using a valve test facility constructed by at ORNL's Engineering Technology Division. The face of each valve was hydraulically loaded until fracture resulted. DDC-supplied valve seats and guides were incorporated in the testing. The strength of valves that were not subjected to engine testing was also examined, and is referred to in the present discussion as "as-received" strength.

The uncensored strength distributions of the as received longitudinally and transversely machined fillet valves were compared. The strengths were higher for the valves whose fillet radius was longitudinally machined (note, the greatest principal tensile stress during both service and laboratory strength testing is located at the surface of the valve's fillet radius). Engine testing the longitudinally machined valves for 166 hours resulted in a decrease in the retained characteristic strength of approximately 26%. Engine testing the transversely machined valves for 1000 hours resulted in a decrease in the retained characteristic strength of approximately 8%. These decreases in strength were not unexpected because past strength and fatigue testing at elevated temperatures using laboratory specimens showed that the strength of NT55 1 decreased. Lastly, the Weibull distributions for these four valve strength sets were compared. It is arguable that the retained strengths of the longitudinally machined valves after 166 hours of engine service were still larger than the strength of the valves whose fillet radius were transversely machined. Fractography was used to identify the strength-limiting flaw in the fractured valves in these four sets, and porous regions, dark-shaded inclusions, and machining damage were the active and dominant flaw-types among the sets.

Strength data from two different test specimen geometries (ASTM Cl 161B and cylindrical bend bars) were used to predict the inert strength failure probability of a NT55 1 DDC Series 149 valve. As a result of (different types of) inhomogeneities in the strength-limiting flaw populations among the specimens and the valves, the life prediction using input from these two flexure specimen data sets did not correlate well to the measured valve strengths. This result reiterates and emphasizes the requirements that ceramic materials must both have the same uniformly distributed flaw population(s) in the test specimen and the component. Unless material homogeneity exists, any meaningful life prediction or reliability analysis of a ceramic component may not be possible.

Publications

1. M. J. Andrews, A. A. Wereszczak, K. Breder, T. P. Kirkland, and M. K. Ferber, "Investigations of the Weibull Modulus as a Function of Stressing Rate," Ceramic Engineering Proceedings, Vol. 19, pp.79-87, 1998.

2. A. A. Wereszczak, M. K. Ferber, T. P. Kirkland, A. S. Barnes, E. L. Frome, and M. N. Menon, "Asymmetric Tensile and Compressive Creep Deformation of Hot Isostatically-Pressed Yttrium Doped Silicon Nitride," Journal of the European Ceramic Society, 19, pp 227-237 (1999).

3. M. J. Andrews, A. A. Wereszczak, and K. Breder, "Prediction of the Inert Strength Distribution of Silicon Nitride Diesel Valves," Ceramic Engineering and Science Proceedings, Vol. 20, 1999.

4. M. J. Andrews, A. A. Wereszczak, T. P. Kirkland, and K. Breder, "Strength and Fatigue of NT551 Silicon Nitride and NT55 1 Diesel Exhaust Valves, " ORNL/TM-1999/332, Feb. 2000.

5. A. A. Wereszczak, T. P. Kirkland, H. T. Lin, and S. K. Lee, "High Temperature Inert Strength and Dynamic Fatigue of Candidate Silicon Nitrides for Diesel Exhaust Valves," to appear in Ceramic Engineering and Science Proceedings, Vol. 21, 2000.

6. A. A. Wereszczak, T. P. Kirkland, H. T. Lin, and S. K. Lee, "Strength and Its Dependence on Secondary Phase Softening in Silicon Nitride," presented at the 102nd Annual Meeting and Exhibition of the American Ceramic Society, St. Louis, Mo, April 30-May 3, 2000.

7. A. A. Wereszczak, T. P. Kirkland, H. T. Lin, and S. K. Lee, "Comparison of Strength and Thermal Properties of Silicon Nitride Ceramics Up to 850°C," to be presented at 'the ASM Materials Solutions 2000 Conference, St. Louis, MO, October 9-12, 2000.

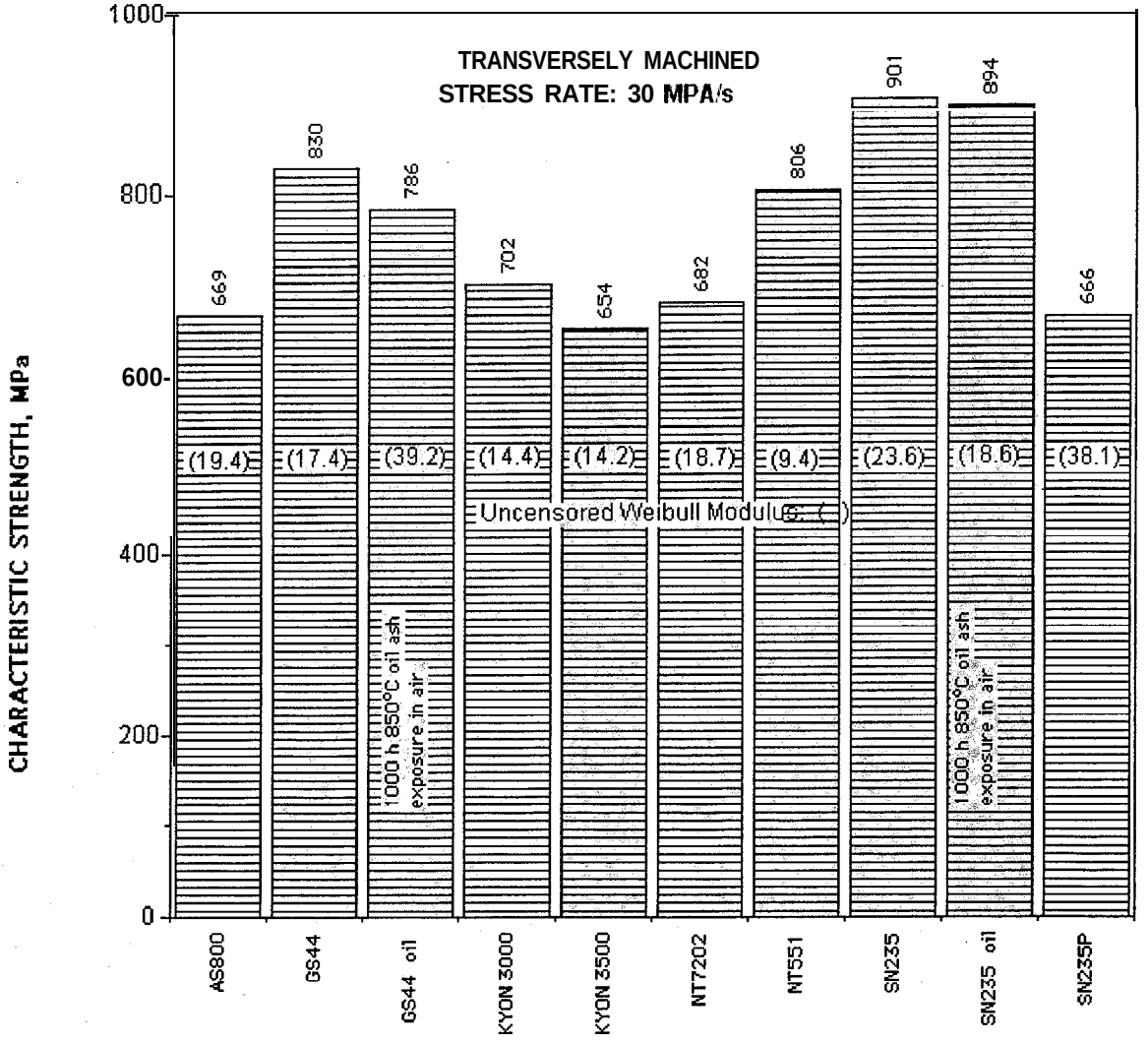

Figure 21. Comparison of the strengths of several types of silicon nitride tested at 20” C.

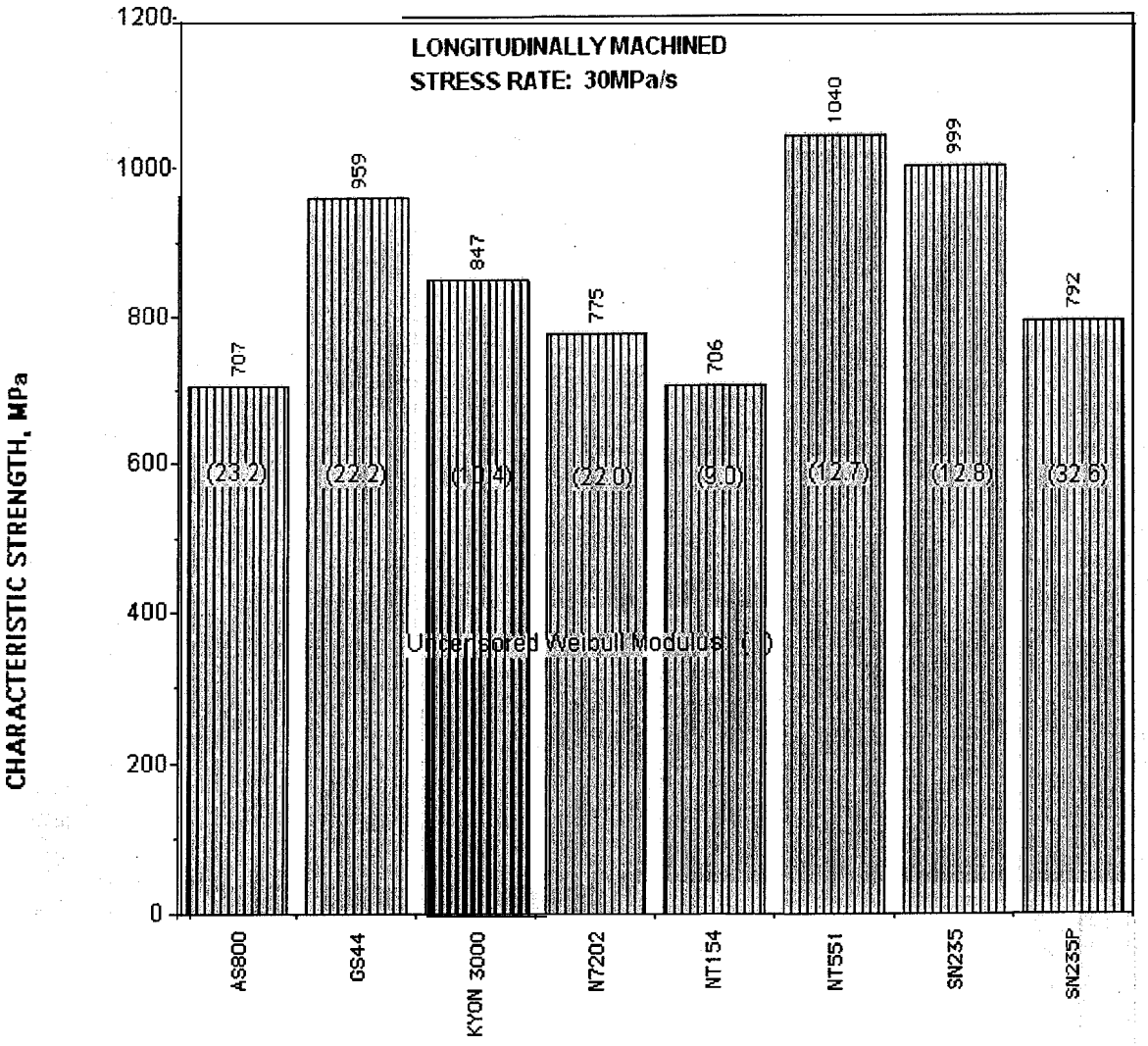

Figure 22. Comparison of the strengths of several types of silicon nitride tested at 20° C.

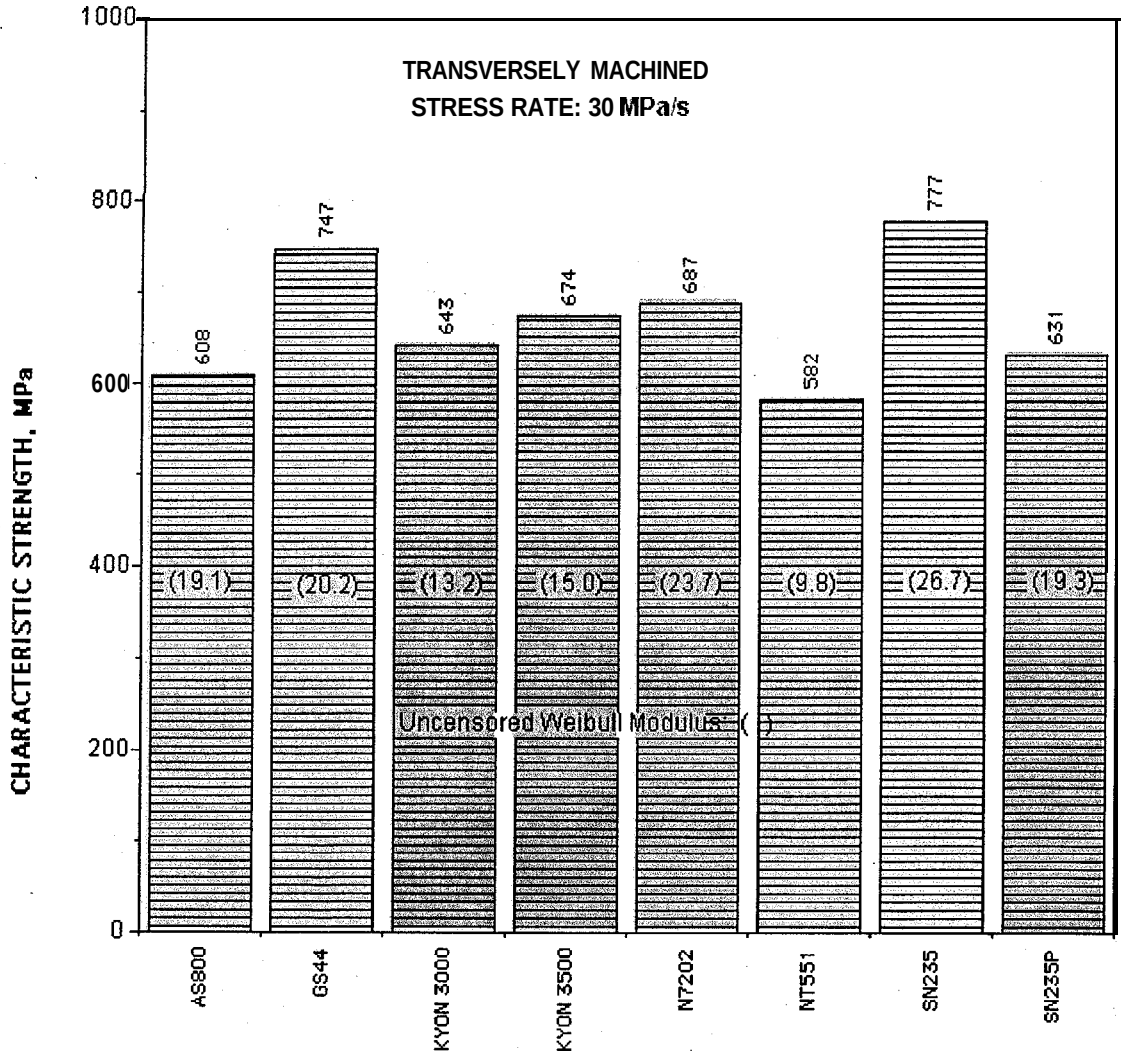

Figure 23. Comparison of the strength of several types of silicon nitride tested at 850° C.

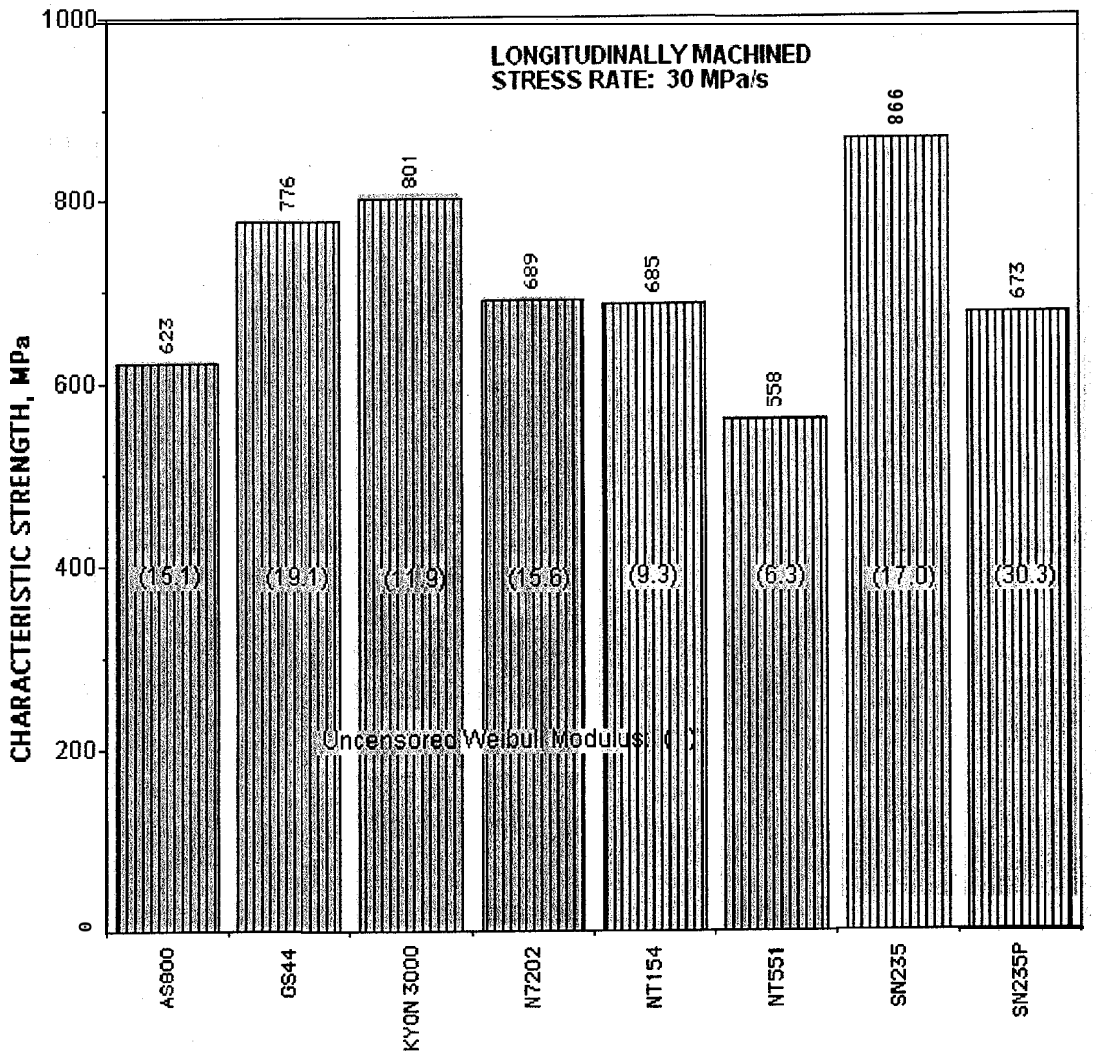

Figure 24. Comparison of the strengths of several types of silicon nitride tested at 850° C.

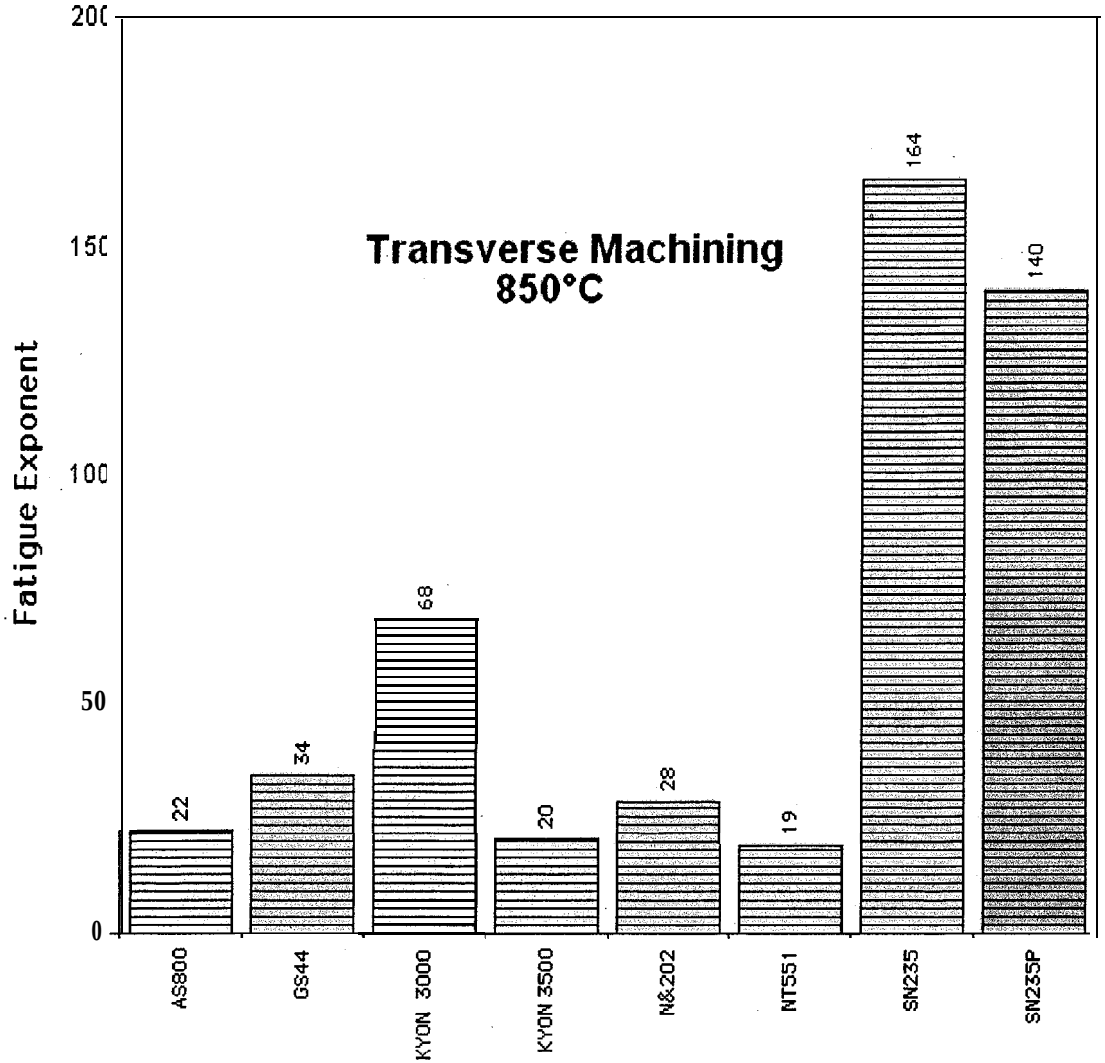

Figure 25. Fatigue exponents for several types of transversely machined silicon nitride.

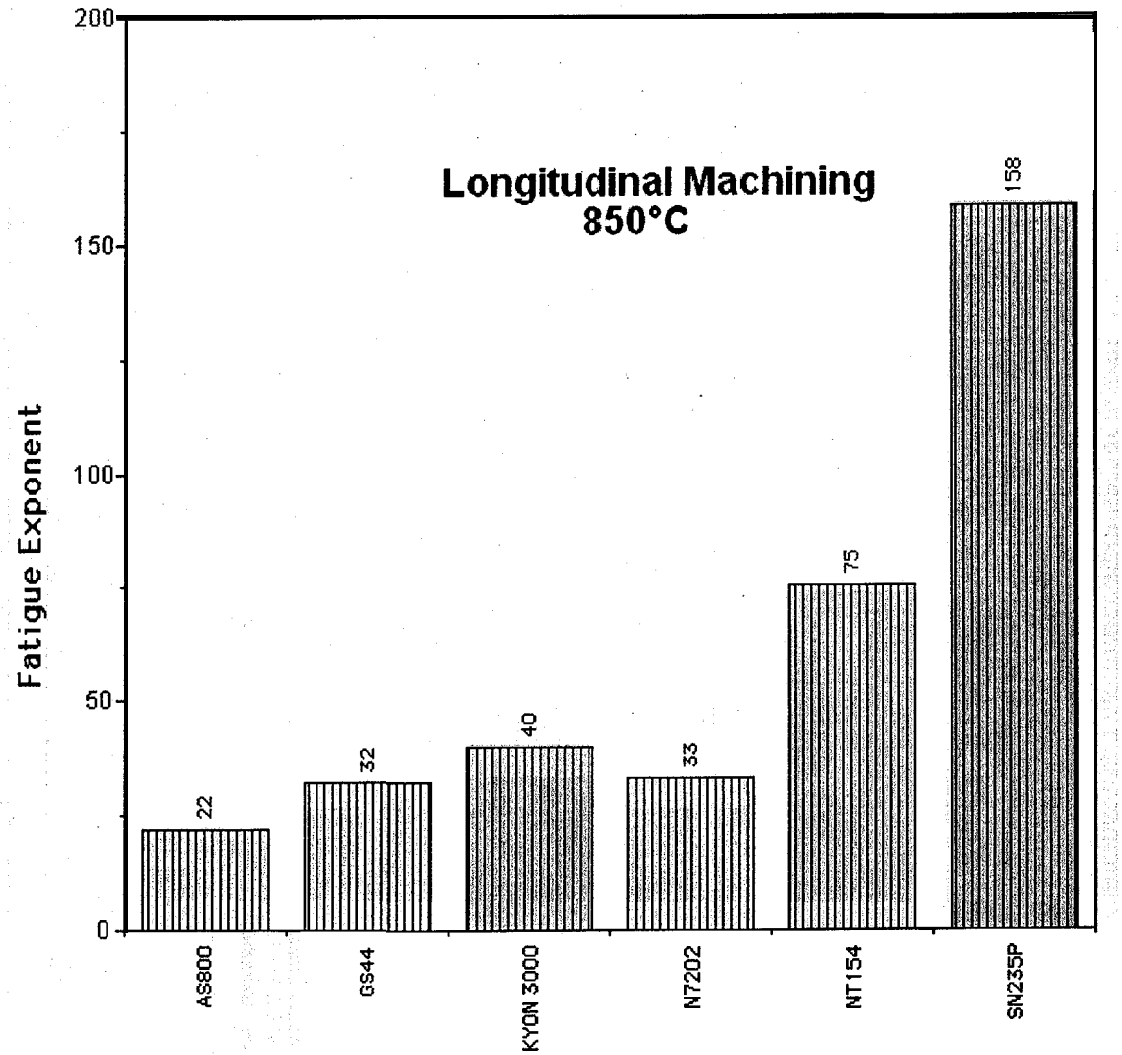

Figure 26. Fatigue exponents for several types of longitudinally machined silicon nitride.

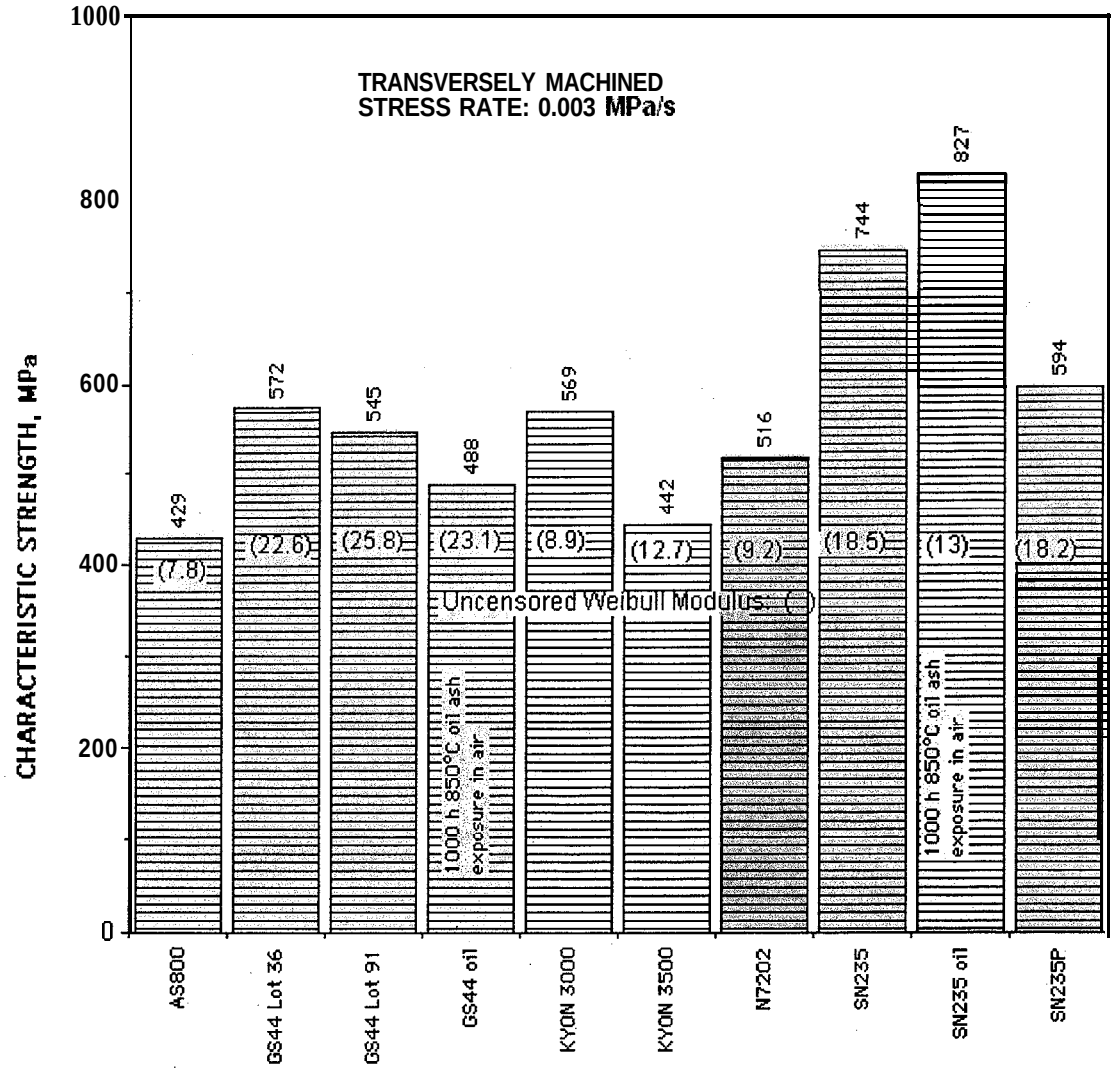

Figure 27. Comparison of the strengths of several types of silicon nitride tested at 850” C.

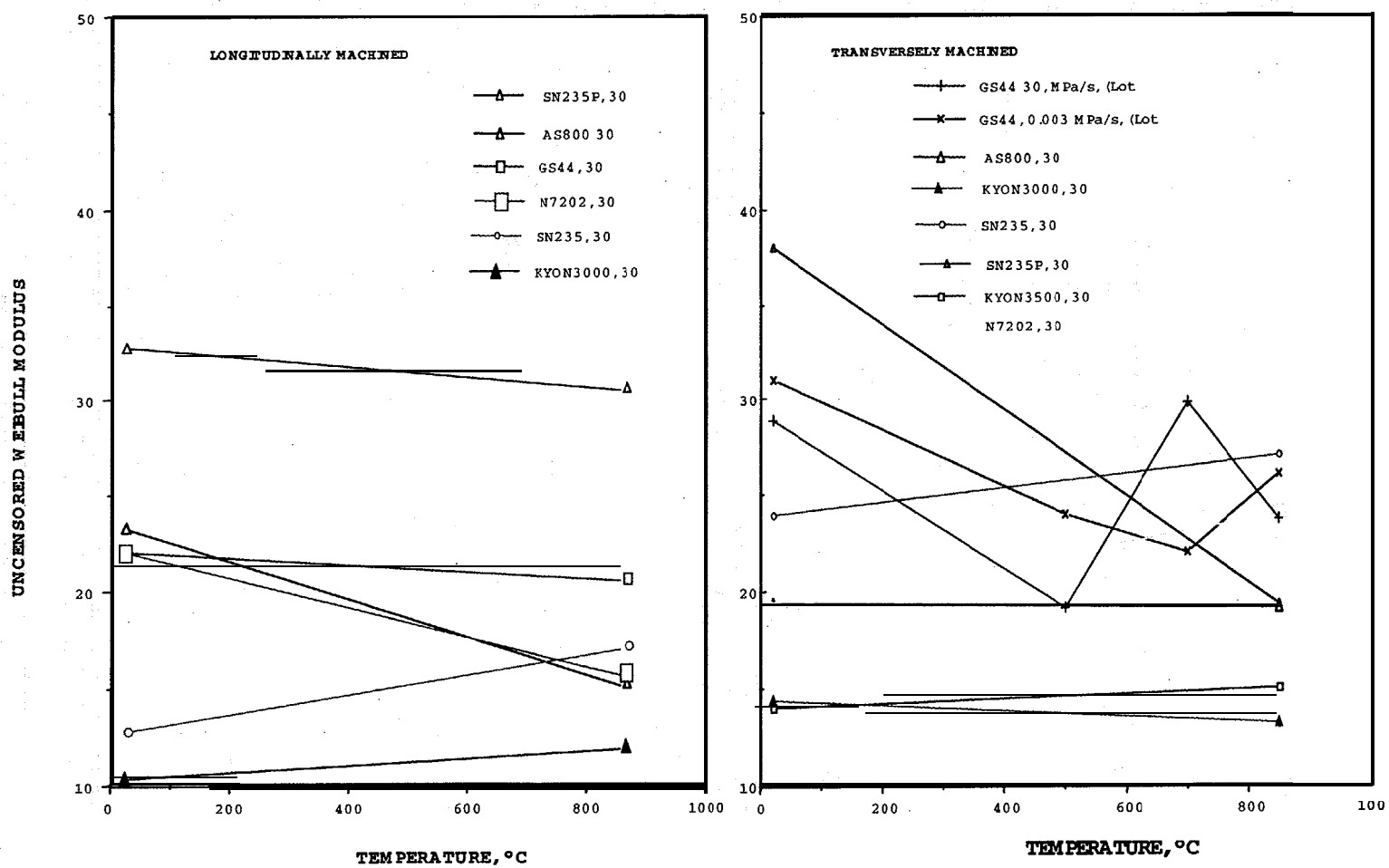

Figure 28. Weibull Modulus as a function of temperature for two machining directions.

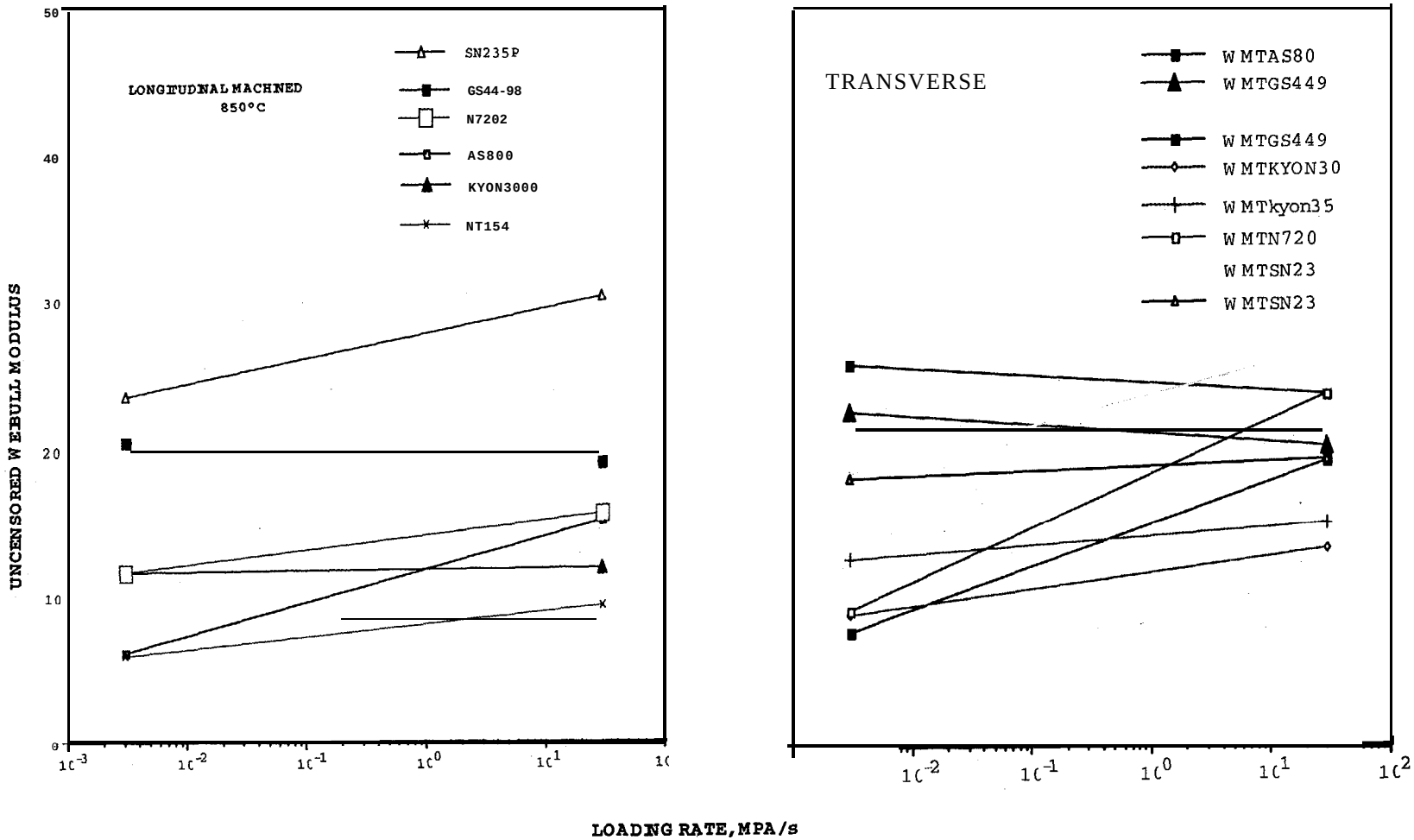

Figure 29. Weibull Modulus as a function of loading rate for two machining directions.

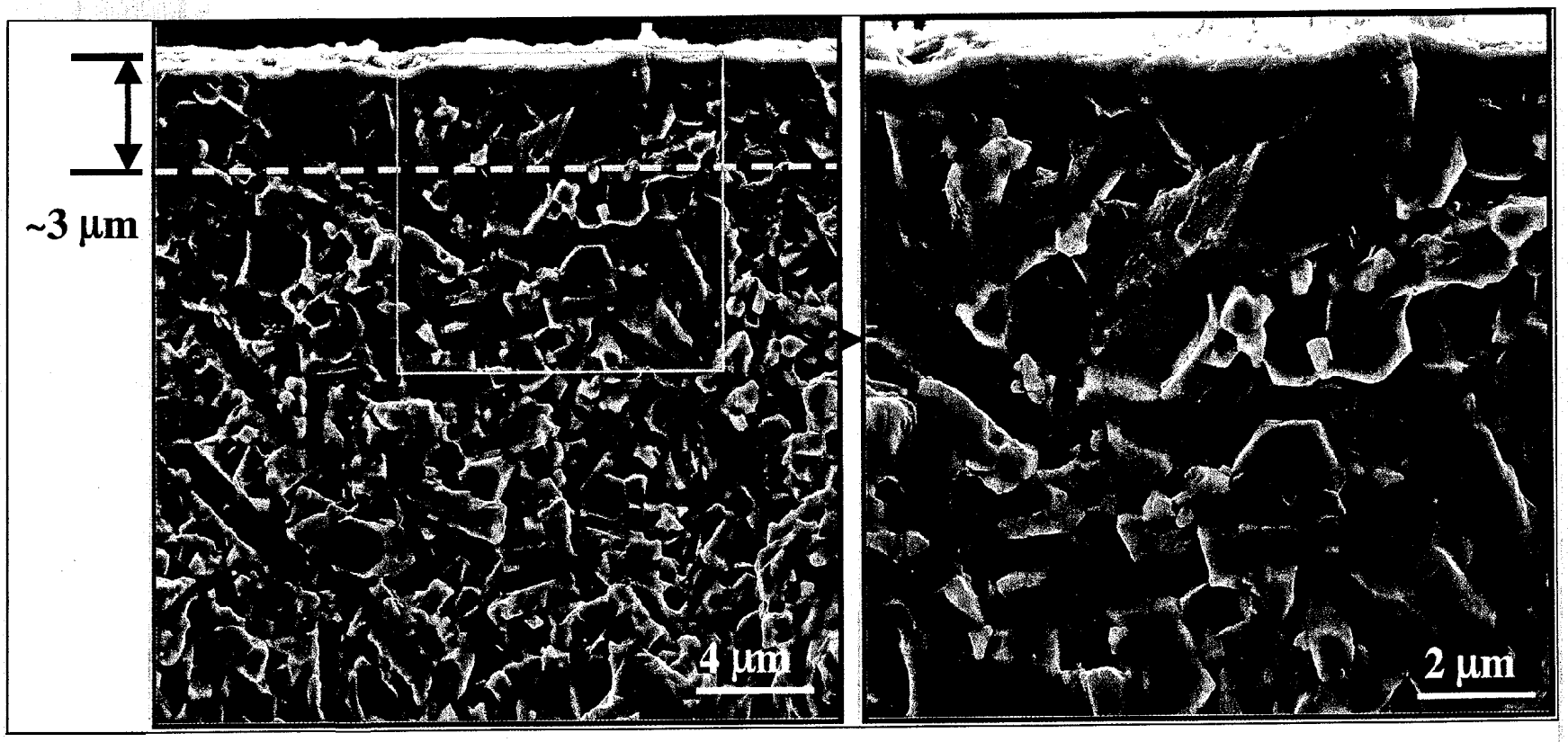

Figure 30. Fracture Surface of Kyocera SN235 After 850°C/1000 h Exposure in Oil Ash Environment

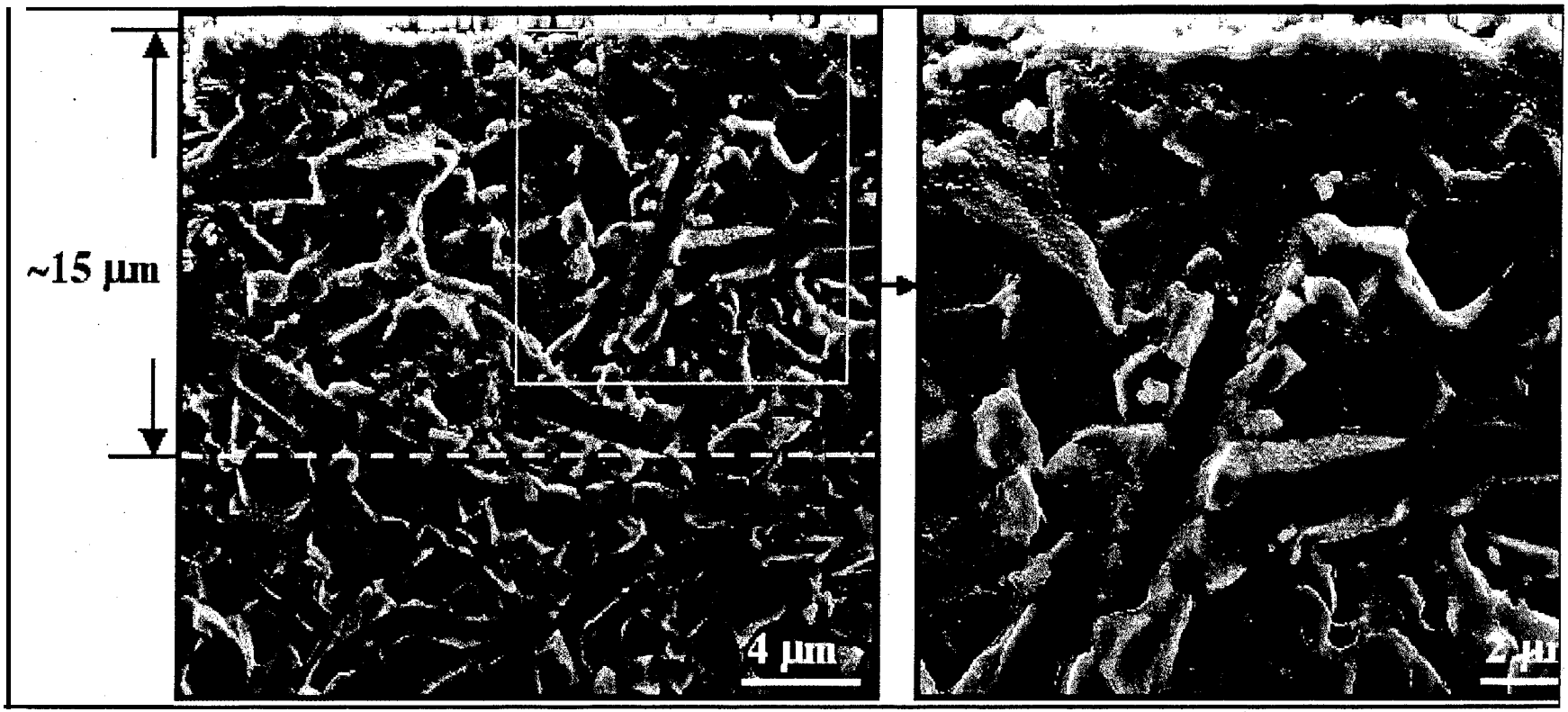

Figure 31. Fracture Surface of Honeywell GS44 After 850°C/1000 h Exposure in Oil Ash Environment.

Task 4 – Residual Stress Studies

Two samples, GS44 plates, machining conditions 1 and 8, were examined using grazing incidence x-ray diffraction (GIXD) with Cu Kα radiation utilizing an incident multilayer mirror and diffraction side radial divergence limiting soller slits. Further, experimental and analysis details can be found in reference 2 below. These samples were machined at high wheel speed/coarse grit and low wheel speed/fine grit, respectively. Early on it was observed in the laboratory that there appeared to be two peaks at low angles of incidence, where one might only expect one (see Figure 32A). The existence of the second peak was confirmed using the high intensity, monochromatic radiation at the synchrotron (see Figure 32B). This second peak has not been reported in the literature.. It is believed that the second high angle peak originates from the plastically deformed Si_3N_4 surface layer. The residual stresses are given in Table 5. Except for position 3, the residual stresses do not appear to vary from point to point on sample #1. The residual stresses are greater in condition 1 than in condition 8, which is not surprising given the machining conditions and previous work.[2]

Figure 33 shows that the stress state approaches equi-biaxial for both samples. Figure 34 and Figure 35 show some of the results of the GIXD experiments. The calculated residual stresses (open circles) for each x-ray penetration depth form the tau profile. The Z profile (solid line) represents an estimate of the actual stress as a function of depth from the sample surface and was deconvoluted from the tau profile. It should be ***emphasized*** that the Z-profiles are estimates and not unique for the data. The reconstructed tau profile (dotted line) was calculated from the solid line and is an estimate of the quality of the solid line. The fit of the reconstructed tau profiles to the original tau profile is reasonable indicating that the Z-profile estimates are good ones.

The tau profiles show the residual stresses decaying rapidly with depth. Here as the depth of penetration was increased the x-ray penetration volume contained more of the material that was either experiencing tension or no stress at all. Thus, the average signal from this volume results in stresses that approach zero, which makes sense considering force balance constraints. A comparison of Figure 34A to Figure 35A and Figure 34B to Figure 35B (Note varied y axis scales!) indicate that the residual stresses in the β-Si_3N_4 were greater in the sample machined with coarser particles. In Figure 34A and Figure 35A, the residual stresses transition from compressive to tensile between 2 and 4 μm. The profiles suggest that the smaller grit transitions closer to the surface.

Table 5. The surface residual stresses from an x-ray penetration depth, Tau, of 0.4 pm.

	Peak 1			Peak 2		
Sample	σ_{11}	σ_{22}	σ_{12}	σ_{11}	σ_{22}	σ_{12}
Condition 1						
Sample 1						
Position 1	-417	-414	15	-2160	-2088	25
Position 2	-419	-457	81	-2131	-2212	155
Position 3	-246	-227	-133	-1907	-1936	-211
Position 4	-407	-280	11	-2032	-1815	-20
Ave	-372	-345	-7	-2058	-2013	-13
STDEV	84	109	90	114	174	152
Condition 8						
Sample 1						
Position 1	-71	-219	-8	-1829	-2055	19

[2] E. S. Zanoria, T. R. Watkins, K. Breder, L. Riester, M. Bashkansky, J. Reintjes, J. G. Sun, W. A. Ellingson and P. J. Blau, "Assessment of Techniques for Characterizing the Surface Quality of Ground Silicon Nitride," ***J. Mater. Eng. and Perf. 7*** [4] ***533-47*** (1998).

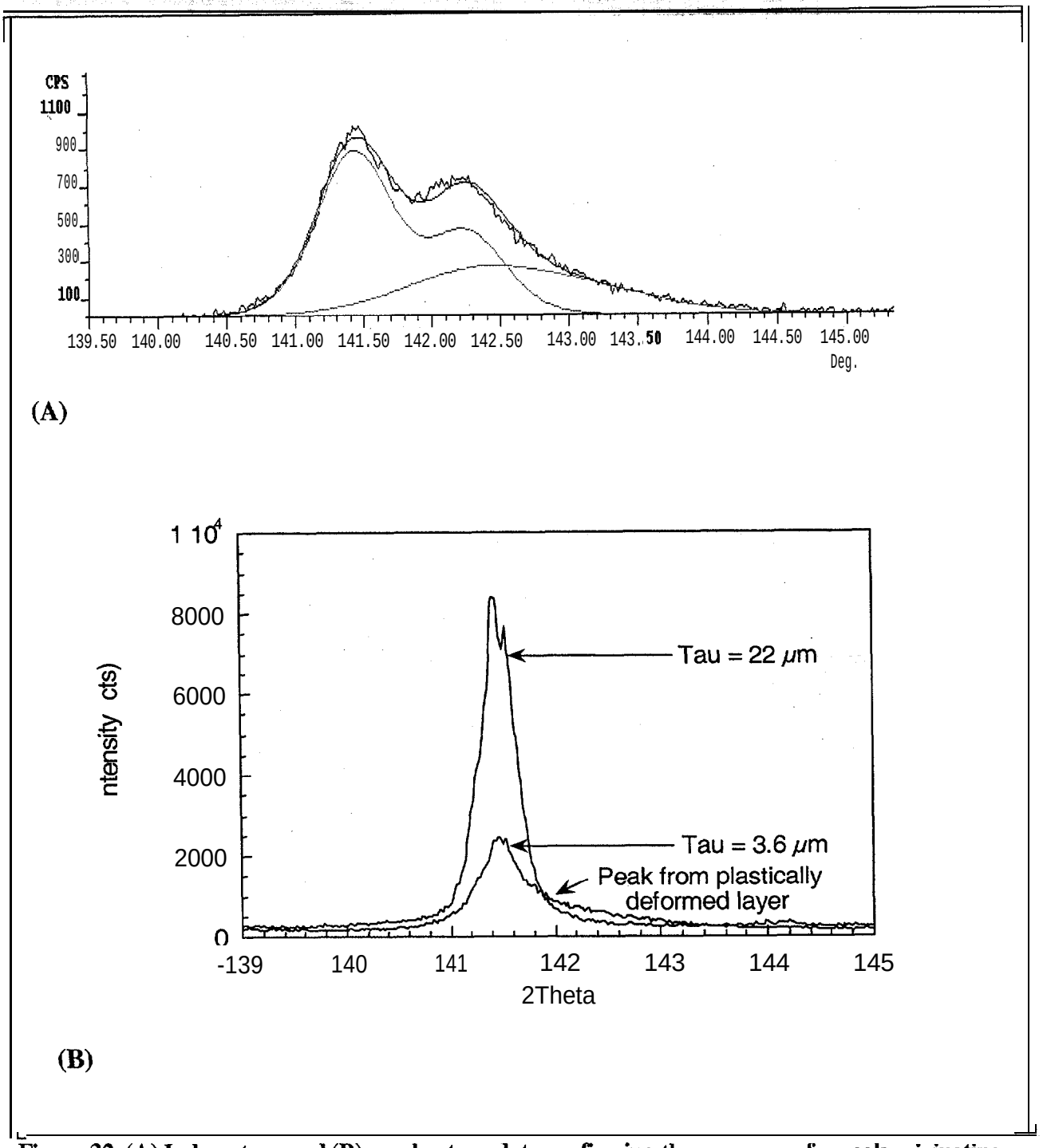

Figure 32. (A) Laboratory and (B) synchrotron data confirming the presence of a peak originating from the plastically deformed surface layer from Sample#1-Condition#1. Peak 1 and 2 are on the left and right, respectively.

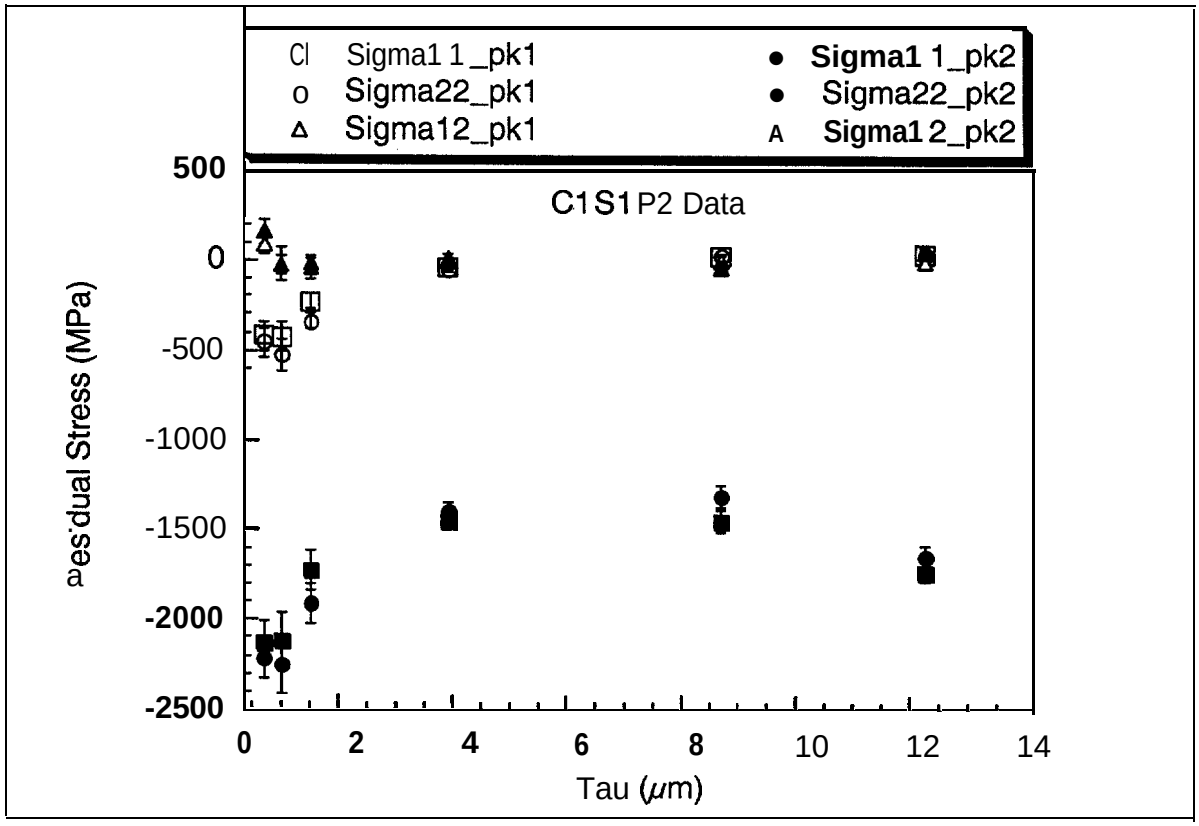

Figure 33. Residual stress parallel to the machining direction as a function of x-ray penetration depth for samples 1, condition 1, position 2, (A) peak 1 and (B) peak 2.

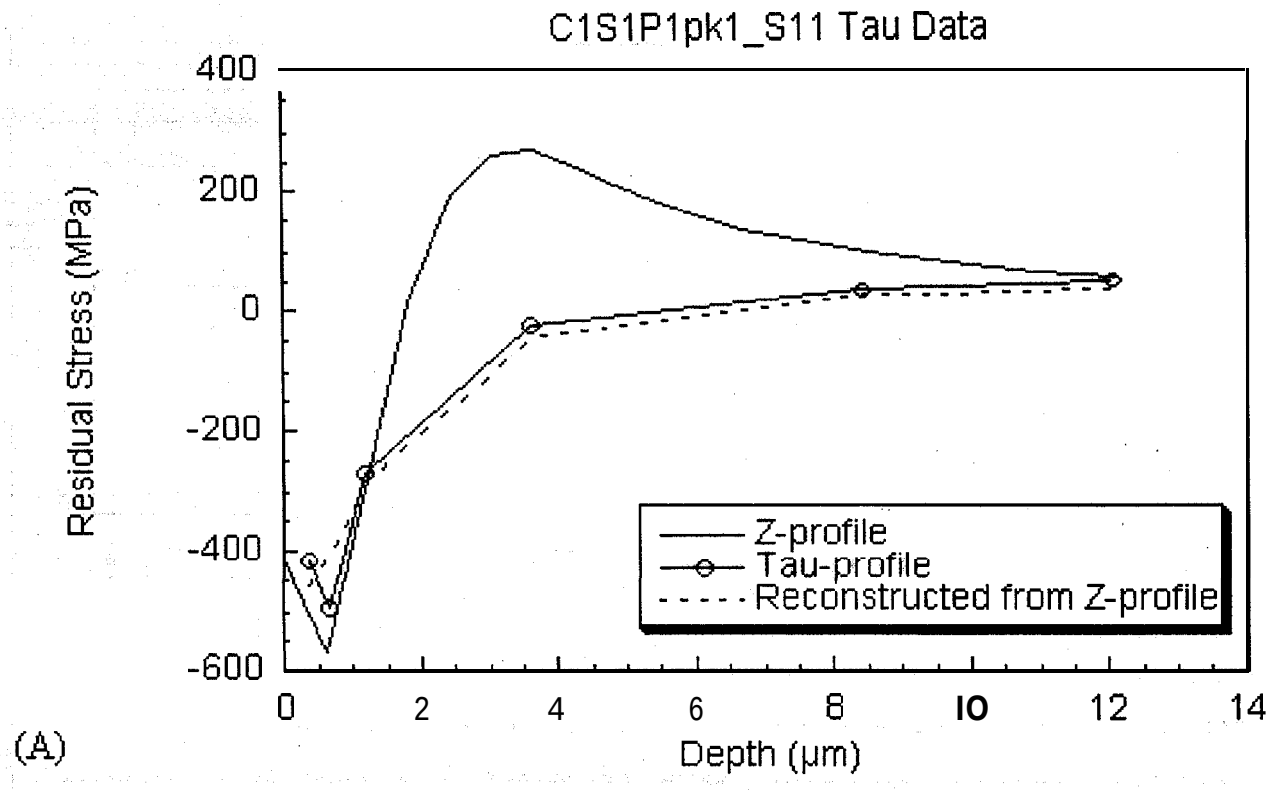

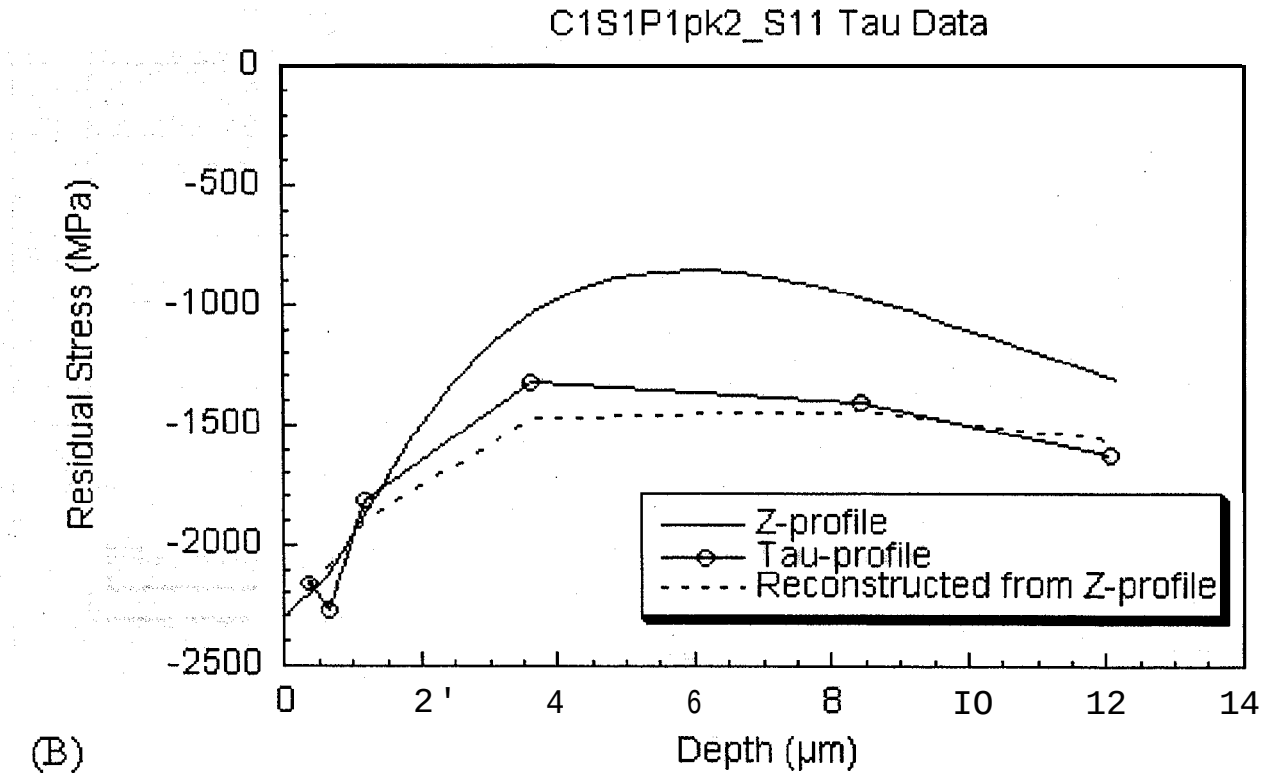

Figure 34. Residual stress parallel to the machining direction as a function of x-ray penetration depth for samples 1, condition 1, position 1, (A) peak 1 and (B) peak 2.

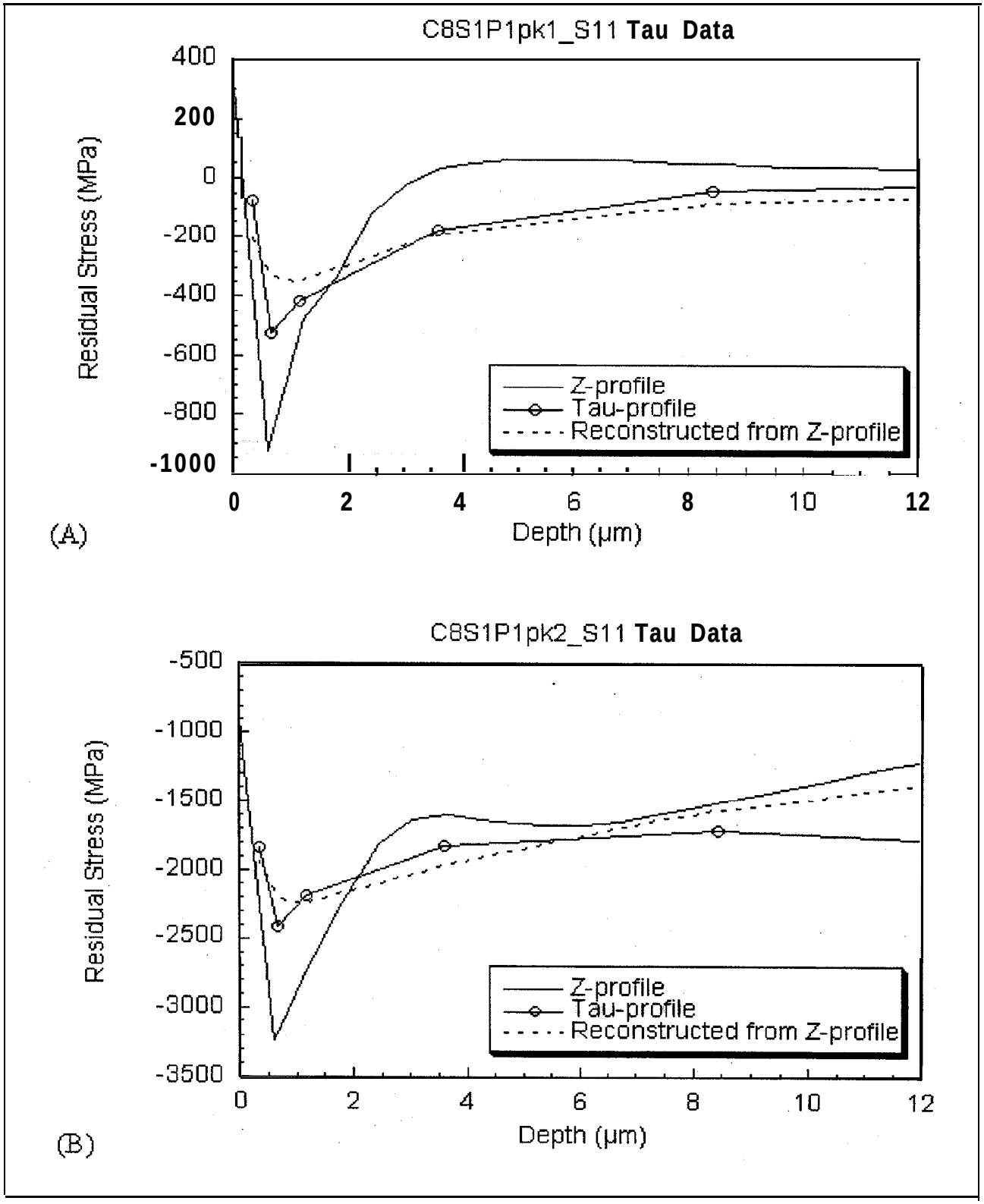

Figure 35. Residual stress parallel to the machining direction as a function of x-ray penetration depth for samples 1, condition 8, position 1, (A) peak 1 and (B) peak 2.

Conclusions and Recommendations

This was a relatively large, multi-year cooperative effort with ambitious goals. In general, the effort was successful, and most of the objectives were fully, or at least partially met. Because of changes in personnel at both Caterpillar and ORNL, it was at times difficult to maintain momentum for the project. However, as can be seen by the data presented in this report, a significant amount of useful information was generated, which should be of interest to both Caterpillar and ORNL.

It is recommended that technical representatives from both ORNL and Caterpillar meet as soon as possible to discuss the outcome of this CRADA and to generate an informal roadmap for future collaborations. It is strongly recommended that such collaborations, which should target the increased use of ceramic materials in diesel engines, should continue. Priority should be given to smaller-scale, shorter-term tasks with specific, clearly stated objectives.

INTERNAL DISTRIBUTION

1. P. A. Carpenter, 4500N, 6269
2. D. R. Johnson, 4515, 6066
3. S. B. McSpadden, 4515, 6069
4. R. D. Ott, 4515, 6063
5. A. E. Pasto, 4515, 6062
6. T. M. Rosseel, 4500S, 6138
7. T. R. Watkins, 4515, 6064
8. P. J. Wenzel, 4500S, 6161
9. K. M. Wilson, 111 UNV, 6499
10. Office of Technical Information & Classification, 4500N, 6254

EXTERNAL DISTRIBUTION

11. M. Andrews, Caterpillar, Inc., Tech Center Building E, 14009 Old Galena Road, Mossville, IL 61552

12. Sid Diamond, Department of Energy, Heavy Vehicle Program, Office of Transportation Technologies, Building EE-33, 1000 Independence Ave, S.W., Washington, DC 20585

13. J. Eberhardt, Department of Energy, Office of Heavy Vehicle Technologies, Building EE-33, 1000 Independence Ave. S.W., Washington, DC 20585

14. B. Fix, Caterpillar Inc., Tech Center Building K, 14009 Old Galena Road, Mossville, IL 61552

15. J. Thiele, Caterpillar Inc., Tech Center Building K, 14009 Old Galena Road, Mossville, IL 61552

16. Andrew A. Wereszczak, U.S. Army Research Laboratory, Weapons and Materials Research, Attn: AMSRL-WM-MC, Aberdeen Proving Ground, MD 21005

1’7. DOE-Work for Others, MS-G209